Influence of Surface Bugholes on Freeze-Thaw Degradation of Tunnel Lining Concrete

トンネル覆工コンクリートの凍結融解劣化におよぼす表面気泡の影響

Dr. Eng. Thesis

by

HU LIANGJUN

**DEPARTMENT OF ENVIRONMENTAL ENGINEERING
YAMAGUCITY UNIVERSITY
UBE, JAPAN
September 2020**

Keywords

Tunnel Lining, Bughole, Freeze-Thaw, Chloride, Image Analysis, Scaling, Surface Penetrant, Silane

Abstract

Bugholes on concrete surface are generally considered as an aesthetic problem. The construction quality of concrete is firstly assessed by surveying the surface appearance. The existence of bughole degrades the surface qualities. Surface bugholes are regarded as an imperfection. An additional surface finishing may increase the construction cost and delays the construction project. In addition, the bughole problems also result in the conflicts of constructors and owners since there is a lack of criteria for numbers and areas of surface bugholes.

Surface bugholes can be mitigated but never eliminated. Surface bugholes often appear on the sidewalls of a tunnel's lining concrete because of the tilting concreting form. The surface bughole could make protentional durability problems, but researchers and constructors commonly ignored it. At the current research, however, the impact of surface bugholes on concrete durability is still unidentified. In cold regions, the lining concrete of a road tunnel is exposed to deicer solutions splashed by traffic, and it is additionally exposed to freeze-thaw (F-T) cycles.

Surface deteriorations such as scaling on concrete happen due to environmental factors such as frost damage and chemical corrosion. Such surface deteriorations in the F-T test are generally quantified by weight loss and/or decrease of dynamic modulus of elasticity. However, it is difficult to examine these properties of huge concrete blocks such as tunnel lining sidewalls. It is hard to quantify local scaling accurately because the current visual inspection methods are based on the slight loss of concrete surface subjected to the scaling. Image analysis has been developed to assess the deterioration of concrete surfaces accurately and efficiently.

Chapter 1 is the introductory chapter of the research work highlighting the bughole problem on concrete surface. The research motivation and scope of the present work have been discussed in detail. In addition, this chapter also includes the layout of the documented work.

Chapter 2 reviews the literature and provides in detail about the surface bugholes, detecting methods of bugholes, F-T damage on concrete, and surface treatments. In addition, this chapter summarizes the literature review and discuss the implications of the literature for the study.

Chapter 3 presents the application of colored image analysis for quantifying the local scaling, as well as the influence of surface holes on local scaling. This chapter conducted an F-T test on mortar specimens with artificial surface holes. The local scaling was quantified by the image analysis based on RGB values in the colored photograph. The results indicate that the image analysis is valid to detect and quantify the area of scaling, including invisible micro-scaling. It was concluded that surface holes negatively affect the scaling of concrete. The surface scaling increases by the initial surface bughole area-ratio. A degradation grade scale based on the area-ratio, including surface holes, is proposed for evaluating local scaling appropriately.

Chapter 4 focuses on the durability of F-T cycles of tunnel lining concrete with surface bugholes. For the objectives, the study was carried out on a laboratory-scale F-T test using large concrete blocks. Image analysis was performed to detect and quantify the deterioration of the concrete surface throughout the F-T cycles. Although severe scaling never occurred during the 300 F-T cycles, the concrete with bugholes indicated a significant local scaling at the edges of the bugholes. Some bugholes enlarged, and some merged with existing bugholes, in accordance with such local scaling. This chapter presents the synergetic and negative effects of bugholes on the local scaling of tunnel lining concrete exposed to F-T cycles.

Chapter 5 focusses on the impact of surface bugholes on chloride penetration of concrete coated with different surface treatments. The chloride penetration of concrete is a crucial concern for reinforced concrete in the saline environment. Although normally tunnel lining concrete is plain concrete, the portal of a tunnel embeds with reinforcement. Various surface treatments are widely used to protect concrete from environmental corrosions. However, surface imperfections, such as bugholes and cracks, may degrade the protective effect of treatment agents. In addition, bugholes' existence may accelerate the process of ingression of liquids and chlorides. Therefore, surface finishing and grinding are required before coating. This chapter was carried on a chloride immersion test. Concrete specimens with different sizes of bugholes were coated with different types of surface treatments. All specimens were immersed in the 3% sodium chloride solution for 100 days. The chloride penetration depth was determined by chromatography method using the 0.1 mol/L silver nitrate solution. The test results show that the silane-based treatment agent has an excellent water-repellent effect even on a concrete surface with bugholes. The penetration depth is increased by

surface hole size when concrete was uncoated or applied with a low water-repellent surface treatment. For concrete applied with high water-repellent surface treatment, the influence of surface bugholes on chloride penetration is negligible. Therefore, finishing or grinding due to surface bugholes is not a must request before coating.

Chapter 6 summarizes the thesis covered so far and concludes the findings in this thesis work. The chapter gives a discussion of the limitations of the research and recommendations for future work.

Table of Contents

List of Figures

List of Tables

List of Abbreviations

F-T	Freeze-thaw
LS	Lithium silicate
NATM	New Austrian tunneling method
R_{A2}	Initial surface bughole area-ratio at area A_2
r_b	Initial surface bughole area-ratio
r_d	Deterioration area-ratio.
r_N	Surface deterioration area-ratio at N freeze-thaw cycle(s)
r_{sN}	Scaling area-ratio at N freeze-thaw cycle(s)
S_d	Total area of pixels estimated as bugholes and scaling in the evaluation area S
S	Evaluation area of a graphical image
SA-LS	Surface penetrant of silane and lithium silicate
SO-LS	Surface penetrant of siloxane and lithium silicate

Statement of Original Authorship

I hereby declare that I am the sole author of this doctoral thesis and that I have not used any sources other than those listed in the references. I further declare that I have not submitted this thesis at any other institution in order to obtain a degree.

Signature:

Date: 2020.08.12

Acknowledgments

Chapter 3 and Chapter 4. These tests took one and a half year, and they both sacrificed their valuable time and gave me great support in my doctoral study.

I am grateful to **Mr. Masayuki Sayama** and **Mr. Shoichi Sayama**, Masaclean Ltd., for their kind assistance on the investigation of surface treatments which was presented in chapter 5. They provided me with an excellent opportunity to broaden my research filed and deepen my research.

I am grateful to **Mr. Takayuki Makihara**, technical staff in the department of environmental engineering, for his continuous technical support and valuable guidance during my study.

I want to thank to all students of Yoshitake lab for their excellent collaboration. They supported me a lot in my research, especially the preparation of specimens and experiments, as well as my daily life in the lab and out of the lab. They were always willing to help me.

I would like to thank my family for supporting me spiritually throughout my doctoral study and my life in general. Mainly, I want to dedicate this thesis to my parents, who always encourage me and support me. Finally, there are my friends, who were a great support in my research as well as provided a happy distraction to rest my mind outside of my research.

<div align="right">2020. 08.12</div>

<div align="right">Hu liangjun</div>

Chapter 1: Introduction

This chapter outlines the background (section 1.1) and research motivation (section 1.2) of the research. Section 1.3 describes the scope of this research. Finally, section 1.4 includes an outline of the remaining chapters of the thesis.

1.1 BACKGROUND

Bughole often appears on concrete surface. The surface bughole is considered as an aesthetical problem and is usually ignored by engineers and constructors. Contractors and owners argue about the surface quality problem since a lack of criteria with respect to surface bugholes in specifics (Reading, 1972). Although constructors have made a lot of effort and took effective means to reduce surface bugholes, for the concrete surface with a negative angle such as tunnel lining sidewall, it is hard to eliminate surface bugholes entirely.

F-T cycles and water absorption are the two major factors of frost damage. Tunnels located in cold areas have different degrees of damage due to F-T cycles from annual climate variations (Kawamura *et al*., 2008; Yu *et al*., 2019). In the cold region, de-icer is spread to prevent icing road. In western Japan, calcium chloride is widely used in the winter season. Water on the roads becomes saline as de-icer mixes with water, and the concrete sidewall of a tunnel lining is susceptible to water splashing due to the vehicle movement. Therefore, lining concrete near the tunnel portals suffers F-T cycles and chloride attack from de-icing materials, which may cause salt scaling and degrade the tunnel structure. The tunnel lining at portals is generally constructed as a reinforced concrete structure (RDA and JICA, 2018). In this case, further steel corrosion may occur.

Surface bugholes cannot be treated equally as pores beneath the concrete surface. Pores can be defined as gel pores, capillary, and air voids according to their size, ranging from nanometres to some milli-meters (Delatte, 2009). Unlike surface bugholes, air voids in the interior of the concrete are a result of the entrained air during concreting (Backstrom *et al*., 1958; Pistilli, 1983). The distance between the voids is regarded as a crucial factor for concrete frost durability (Powers and Helmuth, 1953; MacInnis and Becaudoin, 1968; Mehta and Monteiro, 2006; Valenza and Scherer,

2006). Also, bugholes on the surface, are solely exposed to the environment and directly interact with the surrounding environment.
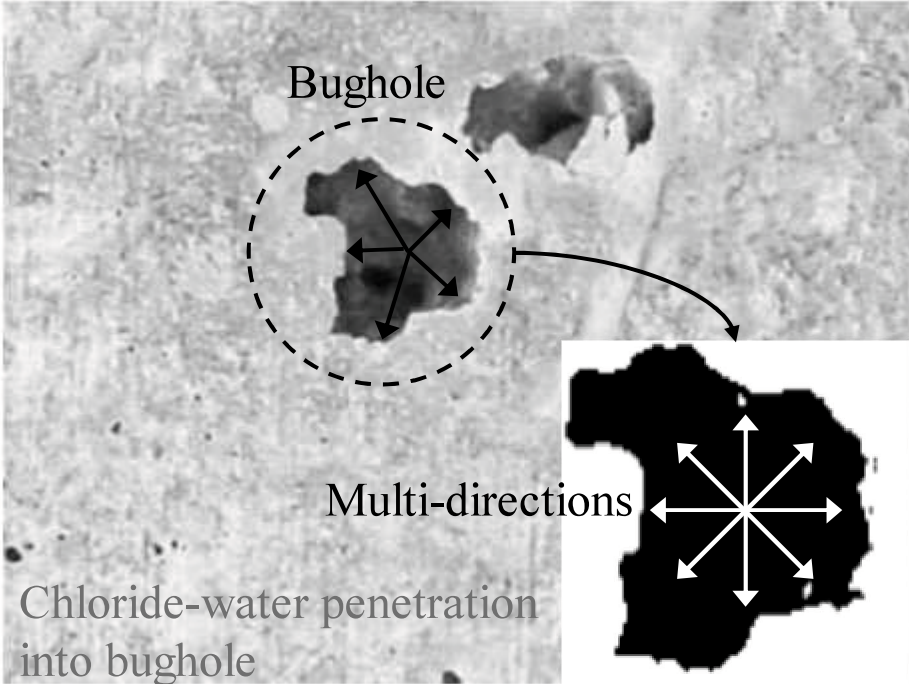
Figure 1-1 Bughole edge subjected to frost attack from various directions

Compared with a smooth concrete surface, bugholes increase the superficial area that is in direct contact with the environment. Consequently, the surface holes hold more adsorbed liquid. A concrete surface is heterogeneous (Sadowski and Mathia, 2016). The concrete surface with bugholes is more heterogeneous than the surface without bugholes, and this may cause further effects on the erosion. The edges of bugholes are affected by the environment from multiple directions. In contrast, a smooth and low-heterogeneous concrete surface is usually affected by the environment in a single direction, as shown in **Figure 1-1**.

Freeze-thaw (F-T) damage of concrete generally happens by surface scaling and internal damage (Pigeon *et al*., 1996; Setzer, 1997). Concrete scaling, progressive removal of small flakes or chips of binder (Valenza and Scherer, 2006), is caused by frost damage, chemical sulfate attack, physical salt attack, and pumping effect (Valenza and Scherer, 2007; Çopuroğlu and Schlangen, 2008; Bassuoni and Rahman, 2016; Liu *et al*., 2018).

Conventional evaluation methods for the F-T damage include weight loss and/or decrease of dynamic modulus of elasticity. However, it is difficult to examine these

properties of huge concrete blocks such as tunnel lining. The grading methods based on the visual inspection are the typical way to evaluate the F-T damage of concrete. However, these visual assessments may be varied by inspectors and may cause subjective and inaccurate evaluation.

Image analysis methods are developed initially to detect deteriorations such as the bugholes. A comparative test conducted by Yoshitake *et al*. (2018) showed that even invisible bugholes (diameter < 1 mm) could be detected in the developed system. With the benefits of high accuracy and efficiency, therefore, the image analysis is widely used to detect surface imperfections.

Various surface treatment materials are used to protect concrete from the harsh environment and to extend the service life of structures. The conditions of the concrete substrate have a significant influence on the penetration depth of penetrants into the concrete. The presence of surface bugholes may cause insufficient coating applications. The engineers worry about the degradation of impregnants due to surface imperfections such as bugholes and cracks. Surface finishing and grinding are required before coating. Thus, construction cost and duration increase due to the additional work.

1.2   RESEARCH MOTIVATION

Researchers have made a lot of efforts to reduce surface bugholes; however, it is hard to eliminate surface bugholes entirely. Especially at tilting form, bugholes remain even after sufficient vibration. The existence of surface bugholes reduces the concrete cover and shortens the distance that chloride needs crossing to arrive at the reinforcement in the RC structure. In the cold region, the bughole area suffers frost damage from multi-directions. In addition, the application of surface treatments may be influenced by surface bugholes. Hence, surface bughole is not a negligible problem. It will probably influence the long-term durability and construction progress.

Mountain tunnels typically constructed by the new Austrian tunneling method (NATM) have a sidewall with a negative angle, where bugholes often appear. Mountain tunnels in the winter season or tunnels in the cold regions suffer cycling climate changes and frost damage. De-icers such as calcium chloride are used to prevent icy road. The portals of these tunnels suffer F-T cycles and chloride attack. The surface bugholes worse the surface condition and degrade the F-T resistance of

tunnel lining. Therefore, the research on potential durability resulting from surface bugholes is needed.

1.3   SCOPE OF WORK

Durability is the most important performance of the concrete structure. Surface bughole is aesthetic related problems, but it also brings potential durability problems. The quantitative evaluation method for surface deterioration is needed to quantify surface deterioration, which is useful in the comparison of the influence factors. This study focuses on the F-T durability of tunnel lining concrete with surface bugholes. This thesis includes the following objectives:

1. To examine the quantitative evaluation method of surface deterioration by image processing technology.

2. To investigate the effect of surface bugholes on F-T durability of tunnel lining concrete.

3. To study the effect of surface bugholes on chloride penetration of concrete coated with penetrants.

1.4   THESIS OUTLINE

Chapter 1: This chapter is the introductory chapter of the research work highlighting the bughole problem on concrete surface. The research motivation and scope of the present work have been discussed in detail. In addition, this chapter also includes the layout of the documented work.

Chapter 2: The literature about the surface bugholes, bughole detections, F-T damage on concrete, and surface treatments have been reviewed and provided in detail in this chapter. Also, this chapter summarizes the literature review and discuss the implications of the literature for the study.

Chapter 3: This chapter describes the image analysis adopted by this research to achieve the aims and objectives that quantitively evaluate the surface scaling on concrete surface. An F-T test on mortar specimens is conducted to examine the applicability of image processing in the quantification of surface deterioration. It compares the visual inspection and image analysis for surface scaling and proposes a deterioration scale based on deterioration area-ratio.

Chapter 4: This chapter presents the synergetic and negative effects of bugholes on the local scaling of tunnel lining concrete exposed to F-T cycles. A laboratory F-T test of 300 cycles was conducted to examine the frost deterioration of tunnel lining concrete. Test parameters included air entrainment agent and surface bughole area-ratio. The surface deterioration area was determined by using image analysis employed in Chapter 3.

Chapter 5: This chapter investigates the effect of surface bugholes on chloride penetration of concrete when concrete is applied with surface treatments. An immersion test was conducted on concrete with surface bugholes in the 3% sodium chloride solution for 100 days. The water absorption and chloride penetration depth were determined. The test results show that the silane-based penetrant has an excellent water-repellent effect even on the concrete surface with bugholes. The chloride penetration depth is increased by surface bughole size when the concrete surface was uncoated or coated with a low water-repellent surface penetrant.

Chapter 6: This chapter summarizes the thesis covered so far and concludes the findings in this thesis work. The chapter gives a discussion of the limitations of the research and recommendations for future work.

Chapter 2: Literature Review

2.1 GENERAL

This chapter reviews literature on the following topics:

Surface bugholes (section 2.2) introduces the definition of surface bugholes and correlated problems with bugholes, including bugholes on tunnel lining sidewall, methods of reducing bugholes, and durability problem resulting from bugholes.

Methods of detecting bugholes (section 2.3) discusses the evaluation methods for surface bugholes, including methods of using photographs as a standard and method of digital processing of images.

Freeze-thaw damage on concrete (section 0) reviews the damage types, influence factors, and basic theories of F-T cycles, and discusses the effect of surface bugholes on F-T durability.

Surface treatments (section 2.5) reviews the types and mechanisms and performance of surface treatment and discusses the impact of surface bugholes on coating application.

Section 2.6 highlights the implications of the literature for the study.

2.2 SURFACE BUGHOLES

Surface bughole is also called surface air voids, blowholes, air bubbles, pinholes (Thompson, 1969; Ozkul and Kucuk, 2011; ACI 347R-14, 2014). These imperfections appear as regular or irregular pits with diameters ranging from few millimeters to 15 mm in diameter and are usually scattered randomly around the surface of the concrete (Ozkul and Kucuk, 2011; Yao *et al.*, 2019). The relation between depth and diameter is not clear because surface bughole is the regular or irregular cavities. ACI 347R-14 (2014) defined bugholes as small regular or irregular cavities, usually less than 0.6 in. (15 mm) in diameter, resulting from entrapment of air bubbles in the surface of formed concrete during placement and consolidation.

Specifications, like ACI 301-05, ACI 301-10, do not show the criterion of bughole size. However, ACI 301-10 gives the maximum size of surface voids. In ACI

301-10, casted surface finishes are grade as SF-1.0, SF-2.0, and SF-3.0. The maximum size of surface voids is 38 mm wide or 12 mm deep for SF-1.0, and 19 mm wide or 12 mm deep for SF-2.0 and SF-3.0, as shown in **Table 2-1**.

<div align="center">Table 2-1 Diameter and depth of bugholes in ACI 301-10</div>

Grade	Diameter (mm)	Depth (mm)
SF 1.0	38	12
SF 2.0	19	12
SF 3.0	19	12

Bugholes problem often considers an aesthetical problem. Bugholes are regarded as a blemish, defects, and imperfections on concrete surface. Sadowski and Mathia (2016) stated the surface of concrete is heterogeneous. The macroscale and mesoscale at which the concrete material is still considered to be continuous but non-homogeneous.

Another problem resulting from bughole is that it led the arguments between the contractor and owner. On the one hand, there was a lack of yardstick for numbers and areas of bughole (Reading, 1972). On the other hand, the existing specifications for surface quality assessment allow for the visual evaluation, which tends to be difficult and evaluation. Those issues can lead to disagreements on the designer-contractor line and project acceptance problems (Thomson, 1969; Kwasny *et al.*, 2015).

2.2.1 Bugholes on tunnel lining sidewall

Tunnels constructed by the NATM are widely located in the mountain area of Japan since the 1970s. NATM is a construction method that integrates the principles of the behavior of rock masses under load and monitoring the performance of underground construction during construction (Kolymbas, 2008). A NATM tunnel is sequentially excavated and supported. The excavation sequences can be changed according to the specific rock condition to efficiently address construction problems being encountered. The initial ground support is provided by shotcrete in combination with fiber or welded-wire fabric reinforcement, steel arches, and sometimes ground

reinforcement. The permanent support is typically a cast-in-place concrete lining (Zhou, 2016).

In addition, it is necessary that the lining concrete thoroughly meets the required requirements of the shape, thickness, material, and workability, and select the most economical concrete materials (JSCE, 2000). Therefore, concrete properties of tunnel lining are generally with a design reference strength of 24 MPa, slump 15 cm, and maximum aggregate dimensions 20-40 mm.

The sidewall of tunnel lining typically has a negative angle, as shown in **Figure 2-1**. Because of the negative angle, bugholes often appear on the concrete surface of the sidewall (Maeda *et al.*, 2014). In addition, the narrow workspace of form makes the vibration and casting work more difficult in the sidewall concreting. **Figure 2-2** shows the typical surface bugholes on a sidewall of tunnel lining concrete. Since a tunnel lining is large volume concrete pours, the maximum size of bughole can be more significant. In this study, the diameter of surface bughole is defined as smaller than 38 mm.
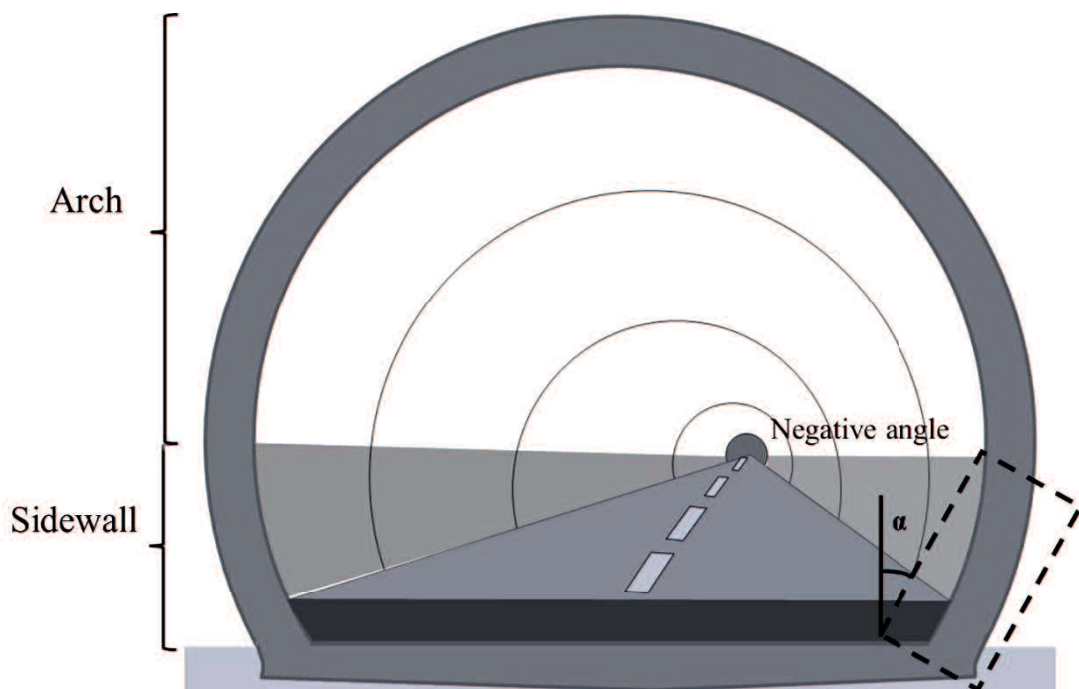
Figure 2-1 Sidewall of a tunnel lining with a negative angle

Figure 2-2 Surface bugholes on the sidewall of tunnel lining concrete
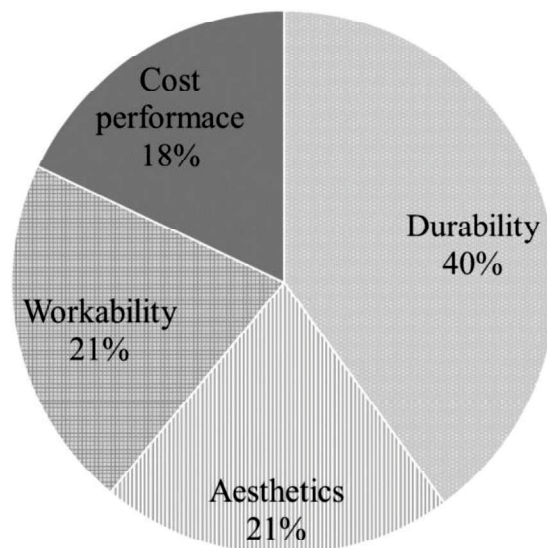
Figure 2-3 The percentage of aesthetics in concrete surface quality
(Hiraoka *et al*., 2012)

Hiraoka *et al*. (2012) made a questionnaire investigation about the surface quality of a tunnel lining. The four factors, including cost performance, workability, aesthetics, and durability, were considered as the assessment requirements in a questionnaire to engineers. **Figure 2-3** shows that the durability of a tunnel lining is the most important factor, but the aesthetics issue occupies an essential position in concrete surface quality.

Yoshitake *et al.* (2012) conducted a questionnaire investigation of surface deterioration of lining concrete in the NATM tunnel. The relative importance of nine typical un-aesthetic phenomena was surveyed, as shown in **Figure 2-4**. The results showed that the air/water bubble took 12% of the aesthetics of lining concrete. It also concluded that "durability" is the most important factor, but "aesthetics" has an almost equal impact of "cost performance" and "workability". The investigation of bughole should not only focus on the aesthetic aspect but also durability influence since durability is the most critical issue.
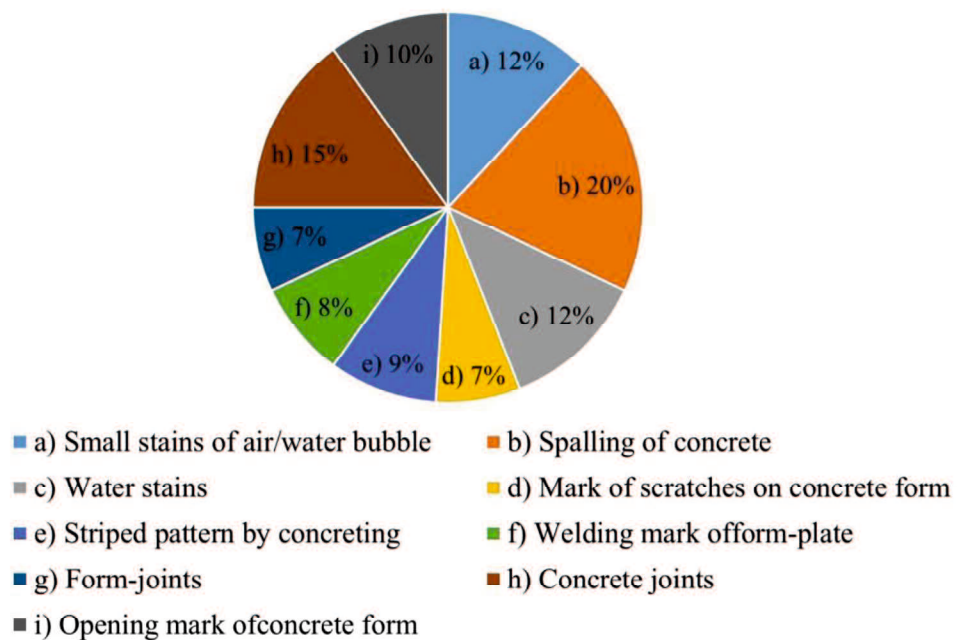
Figure 2-4 Relative percentage of each unaesthetic factor
(Yoshitake *et al*., 2012)

2.2.2 Factors influencing the formation of bugholes

Air is entrapped form oil and entrapped water in the contact surface with the formwork (The SCC European Project Group, 2005). Air bubbles with a diameter of 1 mm and larger are considered as unintentionally entrapped air (ACI, 2010). As much as 20% of the total volume of concrete can be occupied by unintentionally entrapped air introduced during mixing, placing, and compaction process (Neville, 1996).

Stamenkovic (1973) distinguished three types of voids in the concrete surface: water voids, air voids, and attached voids. Houston (1967) and Samuelsson (1970)

reported that air and water bubbles are hardly prevented from slope form during concreting, even after an accurate vibration.

It is important to recognize which factors influence the formation of bugholes on a concrete surface. The influencing factors of mix proportion include water-cementitious material ratio (***w/cm***), superplasticizer (SP) content, sand-aggregate (s/a) ratio, fly ash (FA) content and so on; the influencing factors of construction technology includes remover types, vibration process, and form material (Thompson, 1969; Liu *et al*., 2017b). The appearance of bugholes is noticeable in concrete mixtures with poor filling ability, high viscosity, low slump-flow, and rapid slump-flow reduction (Silva *et al*., 2014).

Reading (1972) pointed out that the properties of the concrete mix affect the degree of success in expelling entrapped air. However, the characteristics of the vibrator and field procedures have an even greater effect. Internal and external vibrators are widely used in concrete vibrations. Internal vibrators should be used in all sections that are sufficiently large for insertion and manipulation. Internal consolidating vibrator of long duration and high frequency can remove entrapped air more efficiently; however, it is hard to eliminate bugholes entirely (Popovics, 1973; Houston, 1967; Samuelsson, 1970; Kwasny *et al*., 2015). It is nearly impossible to eliminate air voids from inwardly slopping formed surfaces (Reading, 1972; Houston, 1967). Hirano *et al*. (2015) point out that bugholes significantly increase in the case of 30 degrees or greater negative angle of concrete form. During the vibration, water bubbles and air bubbles, as the lightest elements in the concrete mass, tend to flow toward the most fluid center of gravity, where the vibrator is located. Where internal vibration is used, the drops and bubbles move up and get out in the immediate vicinity of the vibrator. External vibrators include form vibrators, vibrating tables, surface vibrators, and so on. With external vibration, the water/air bubble tends to adhere to the form. For this reason, the vibration of outside forms, with simultaneous pounding or hammering of the forms, will diminish the volume and total area of the surface voids. Stamenkovic (1973) reported that hammering benefited to the removal of surface voids as well as increase the strength of concrete.

Kwasny *et al*. (2015) reported that an increase in the yield value caused the increase in bugholes content (diameter < 1 mm). It was more pronounced for bugholes with a size smaller than 1 mm. Once the vibration was ceased, the build-up of shear

stress began, gradually slowing down the upward movement of air bubbles and eventually preventing their escape to the top surface of the concrete. Moreover, Silva *et al*. (2014) declared that a reduction in the concrete shear stress ratio contributed to reducing the percentage of bugholes.

The aesthetics of a concrete surface is directly correlated with the type of concrete/formwork interface (Libessart *et al*., 2014). Liu *et al*. (2017b) reported that compared with wood formwork, the concrete surface using steel formwork and PVC formwork has a higher amount of small bugholes and lower bughole area ratio, but the influence of formwork on the maximum diameter of bugholes on the concrete surface is not significant. The concretes with a different slump, mold release agents, and formworks need different vibration time in order to decrease the bugholes on the concrete surface. Price and Widdows (1991) compared the surface properties of concretes cast in both conventional (impermeable) formwork and in permeable formwork, and the use of permeable formwork had greatly reduced the incidence of bugholes on the formed surfaces. Harada *et al*. (2015) and Maeda *et al*. (2016) used permeable sheets to reduce the formation of bugholes on the concrete surface of tunnel lining sidewall. The permeable sheet is effective in decreasing the bugholes (Cairns, 1999; Shyha *et al*., 2016) while it may negatively affect the color of the concrete surface.

2.2.3 Durability problem resulting from bugholes

Researchers have different opinions about the effect of bugholes on concrete structure and service life.

Yoshitake *et al*. (2012; 2018) reported that surface bugholes on the sidewall of a tunnel lining only cause aesthetics effects but do not significantly degrade the structural performance. Ozkul and Kucuk (2010) stated that bugholes are cosmetic surface imperfections and do not affect the structural integrity of the concrete structure.

Bughole has been recently considered as a durability problem in addition to the aesthetical problem. Maeda *et al*. (2014) examined the permeability of concrete with surface bugholes by the Torrent method. Their test results showed that the relation is a logarithmic curve of the bughole area-ratio and gas permeability. An increase of permeability coefficient caused by bugholes, may accelerate the ingress process of

liquids and affect the long-term durability of concrete (Mehta and Monteiro, 2006; Benito Saorin *et al*., 2018).

Setzer (1997) and Benito Saorin *et al.* (2018) mentioned that surface finishing of a concrete element might relate the external and internal porosities with the mechanical and durability properties and has a significant effect on the scaling resistance of a concrete surface. Sadowski and Mathia (2016) stated that the properties of the near-surface layer influence the barrier properties of concrete and its durability in consequence. Also, bughole shortens the distance, which chlorides need to cross from cover-concrete to the reinforcing bar and increases superficial area. Hence, it is necessary to investigate the effect of surface bugholes on durability.

2.3   METHODS OF DETECTING BUGHOLES

Thompson (1969) stated that finding a suitable standard of reference is one of the first problems associated with any discussion about blowholes. A yardstick is a need for evaluation of bugholes on the concrete surface if we want to discuss different types and degrees of formation of blowholes that may be compared. This reference may form a basis for the specification.

Due to the influence of surface bugholes on the appearance quality of concrete, the method for the detection and evaluation of surface bugholes had been established very early. In terms of objects, they can be classified into two categories: methods of using photographs as a standard and method of digital processing of images.

2.3.1 The methods of using photographs as a standard

The method of using photographs as a standard has been adopted in preference to a number of more sophisticated methods which were based on the measurement of diameters and areas of holes. It is much simpler and is generally satisfactory.

Thompson (1969) proposed a set of 10 photographs of concrete surface bugholes as a standard reference (**Figure 2-5**). He described a surface quality of finish by using the percentage area of the concrete surface covered by one or more photographs. Conseil International du Batiment (CIB) (1973) gave a reference bubble scale to classify concrete containing bugholes (**Figure 2-6**). They inspected a concrete element and compared it with the standard templates. CIB W29 is the simplest method found, although it does not quantify. However, the CIB W29 method leaves room for some

subjective appreciation (Lemaire *et al.*, 2005). The detailed survey is a conventional and reliable way to detect bugholes, which requires many human resources and has a long inspection time (Yoshitake *et al.*, 2018). It is a labor-intensive method. These conventional methods have hardly been used in the evaluation of bughole distributions on tunnel linings because of their relatively long and wide concrete surfaces under low lighting conditions.
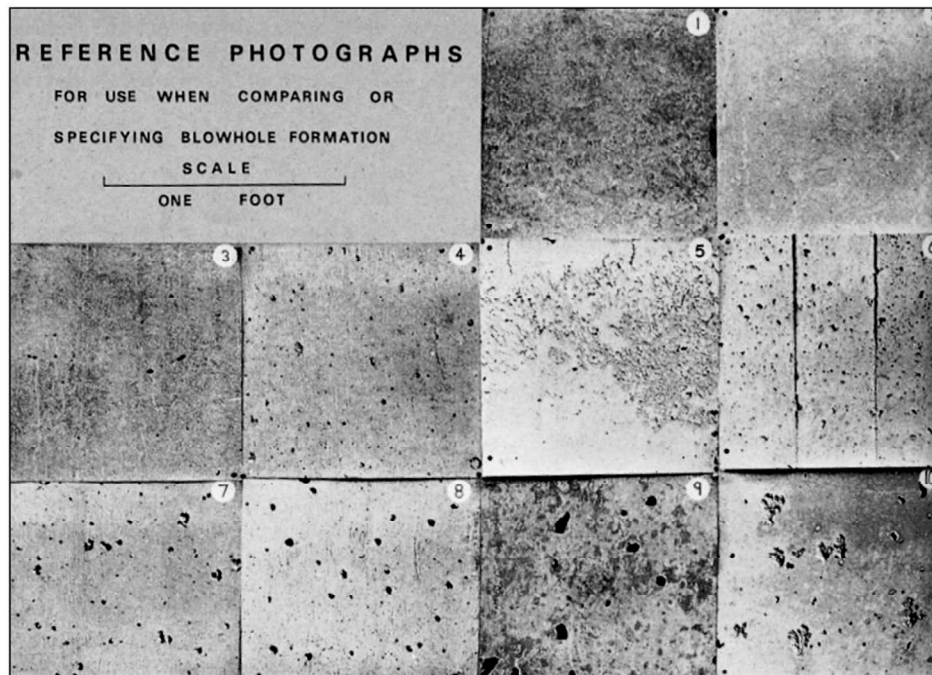
Figure 2-5 Reference photographs used for comparing surface finishes
(Thompson, 1969)
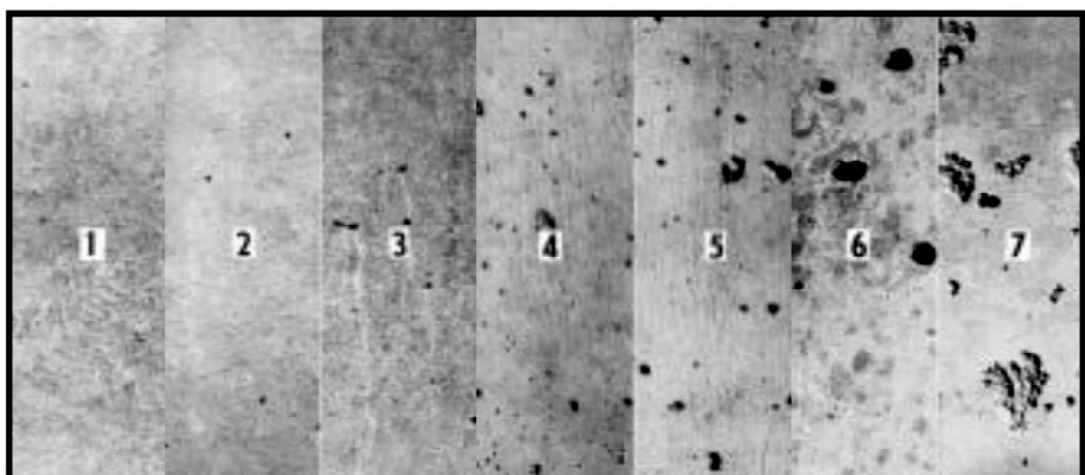
Figure 2-6 Bughole scale
(CIB W29, 1973)

2.3.2 The digital processing of images

According to premises of quality introduced into the control software, the digital processing of images allows the zones with surface defects to be delimited and quantified (Benito Saorin *et al*., 2018).

Lemaire *et al*. (2005) employed the CIB reference and performed an image analysis to examine the bughole size and defect distribution. Not only can the results be compared with current standards (CIB W29), but the method also gives access to additional, accurate information such as the distribution of defects and the size of surface bubbles.

Ozkul and Kucuk (2010) developed a device utilizing the pressure differential technique to measure bughole rating the quality of a concrete surface. The percentage of bughole areas detected by the device was comparable to the result of image analysis presented by Lemaire *et al*. (2005).

Silva and Štemberk (2013) reported a combined image analysis technique and a fuzzy logic-based classification system for assessing the quality of self-compacting concrete surface. The system classifies the surface condition according to the presence of bugholes. The classification considers the bughole percentage area, diameter, and distribution.

Kwasny *et al*. (2015) examined the effects of the rheological properties of mortars on the surface finish. They confirmed that an increase in applied vibration contributes to the removal of bugholes. The original color photograph was transformed into a binary image, and the content of surface air voids was calculated by dividing the area covered with white color (surface air voids) by the area of the tested section.

Peterson *et al*. (2009) discussed a thresholding method based on the image analysis of a concrete surface. They used a flatbed scanner connected to a personal computer and analyzed images to detect air voids. The optimum threshold determination is ultimately derived from the opinions of a human operator. The demerit is that the involvement of a human operator begs the question of whether the operator was right or wrong during their assessment of the sample.

Zhu and Brilakis (2008) developed an inspection methodology for detecting bugholes quantitatively and automatically. The methodology is implemented in a C++ based Prototype and tested on a database of concrete surface images. Comparisons

with manual tests validated its measuring accuracy. As a result, they gave a methodology that can increase the reliability of concrete surface quality assessment. Furthermore, Zhu and Brilakis (2010) presented an inspection system that detects bugholes and the discoloration of a concrete surface. The number of bugholes and the area of regions of discoloration are automatically calculated by the system, and the concrete surface quality can be evaluated using a threshold.

Rashidi *et al.* (2010) conducted a comparative study of machine learning techniques for image processing analysis. They reported that the support vector machine (SVM) classifier has higher accuracy for detecting the material color and textures in images.

Liu and Yang (2017a) established a detection method of concrete bugholes using the image processing toolbox of MATLAB. They proposed an empirical equation based on the relationship between the CIB scale and the bughole area-ratio. The bughole area-ratio can be obtained by using detection software. According to the existing regulation (MOHURD, 2009) and the CIB classification, seven-levels of the surface quality can be obtained, as shown in **Table 2-2**.

Table 2-2 Classification of bughole (Liu and Yang, 2017)

CIB scale	1	2	3	4	5	6	7
Bughole area-ratio (%)	≤0.1	≤0.3	≤0.6	≤1.2	≤2.5	≤5	≤0.7
Maximum diameter (mm)	≤2	≤4	≤6	≤8	≤10	≤12	≤14

2.4 FREEZE-THAW DAMAGE ON CONCRETE

Tunnels located in cold areas and mountain areas have different degrees of damage because of annually cycling climate variations. Cold Regions include all the permafrost area, the glacier area, and the great majority of stable seasonal snow cover area (Chen *et al.*, 2006).

Kawamura *et al.* (2008) measured the tunnel temperature field in the north of Japan and presented a theoretical equation for estimating the temperature in the tunnel. This equation considered heat convection/conduction between the tunnel ground and the airflow in the tunnel. The average temperature and average amplitude vary by the distance from tunnel portals. Chen and Luo (2008) reported that the variation rule of

yearly temperature in the tunnel was periodical, basically accords with the sine curve. Vertical yearly temperature and shake amplitude decrease gradually with the increase of the distance entering a tunnel, and the changing rule was exponent curve. The calculated values were amended according to the altitude of the tunnel portal to obtain the annual average temperature and the annual temperature amplitude of the tunnel portal (Luo *et al.*, 2010). Yu *et al.* (2019) presented three-dimensional numerical simulations of tunnel temperature fields at different temperature conditions. They studied the tunnel temperature field in two different conditions with relatively low (-20 ℃) and high ambient temperatures (30 ℃) representing winter and summer of northeast China. Nearly full length of the lining is affected by ambient temperature. In winter, the temperature of the lining near the tunnel entrance is close to the ambient temperature.

Huang (2003) analyzed the variation regularity of temperature field around the freezing and thawing lithosphere of permafrost tunnels. It was found that the influence of air temperature in the tunnel on the rock mass temperature decreased with the increase of the depth of rock mass. Luo and Chen (2019) reviewed the problems of frost damage in cold region tunnels.

Luo (2010) made a classification of tunnel cold degree, based on the average temperature of the coldest month and freezing depth. Meanwhile, combined with the groundwater conditions, frost damage levels were divided into five using a comprehensive evaluation method. In addition, he proposed that the hazard degree of groundwater to tunnel frost damage should be quantified in further study to realize a reliable and feasible classification.

Frost damages on concrete can be defined as occurring in two major types: scaling of the binder from the concrete surface and internal damage of the concrete (Pigeon *et al.*, 1996; Setzer, 1997). Both field experience and laboratory tests have revealed that internal cracking in properly air-entrained concretes due to frost is almost non-existent. Concrete scaling, the progressive removal of small flakes or chips of binder (Valenza and Scherer, 2006), can be caused by frost damage, chemical sulfate attack, physical salt attack, and pumping effect (Bassuoni and Rahman, 2016; Çopuroğlu and Schlangen, 2008; Liu *et al.*, 2018; Valenza and Scherer, 2007).

The requirements and test methods on frost resistance of concrete vary from country to country. TC 117-FDC recommended the CDF test (capillary suction of

deicer solution and freeze-thaw test) for the determination of the scaling resistance of concrete (RILEM, 1993; Setzer *et al.*, 1996). Note is that types of dicers, concentrations of the solution, presence of free liquid (Valenza and Scherer, 2007) have significant effects on frost scaling. The decline of the concrete surface quality caused by salt scaling makes the appearance porous and results in the creation of pits and craters.

Salt scaling is a severe problem in cold regions due to F-T cycles and the existence of salt water, where deicer is widely used to prevent icy-roads. The edges of the surface bugholes are exposed to frost attack from various directions, as shown in **Figure 1-1**. The bugholes on sidewalls of tunnel lining may make salt scaling worse due to local scaling.

Detecting the weight loss and the decrease of dynamic modulus of elasticity are the conventional evaluation methods for the F-T damage. But for huge concrete blocks such as tunnel lining and bridge piers, it is difficult to examine these properties. Therefore, visual inspections are used to assess the surface quality of concrete. The visual evaluation methods of surface scaling are discussed in section 3.1.

2.5 SURFACE TREATMENTS

Surface treatment materials are useful to prevent liquids and gas penetration and extend the service life of structures. They are widely used to protect concrete from the harsh environment, such as the marine environment.

According to the chemical composition, surface treatments can be classified into inorganic and organic treatments. In terms of functions, surface treatments are divided into three major types: hydrophobic impregnation, impregnation, and coatings (Pan *et al.*, 2017a). Silicate-based penetrants are typically inorganic surface treatment and impregnation of sealing agents, such as lithium silicate and sodium silicate. They are practical to block capillary pores in concrete surfaces and makes concrete densification by reacting with calcium hydroxide and producing insoluble CSH gel (Ca–SiO2) (Kasselouri *et al.*, 2001; Moon *et al.*, 2007; Bertolini *et al.*, 2013; Park *et al.*, 2014). Siloxane and silane are hydrophobic penetrants, which can penetrate concrete pores and make concrete against water and water-born ions (Pan *et al.*, 2017a). By surface impregnation of concrete with silane or adding silane to fresh concrete (integral water

repellent concrete), capillary absorption can be practically suppressed (Wittmann, 2007; Zhu *et al.*, 2013; Ma *et al.*, 2016; Ma *et al.*, 2018).

Increasing the thickness of cover concrete is an effective way to protect concrete from environmental deterioration. But it will be effective only when it increases the cover concrete to centimeters. That will increase the self-weight of structures, influence the structural performance, and cause a higher cost compared with using surface treatments.

The influencing factors for the cost of surface coating includes:

a. Size of area: Big area, higher cost.

b. Complexity of structure: High complexity, higher price.

c. Surface preparation requirements: Surface requiring special preparation and finishing will cost more. If surfaces do not require cleaning and preparation, then the cost will be less.

The types and environment effect the capacity of surface treatment to protection. It should be noted that the durability of surface treatments has significant impact on the durability of surface-treated concrete. The durability of the surface treatments is influenced by temperature cycle, dry-wet cycle, and radiation etc. (Basheer *et al.*, 1997; Eymard *et al.*, *2015;* Li *et al.*, 2015; Kozak, 2015)

Table 2-3 Service-life prediction of coatings under natural environment
(Li *et al.*, 2015)

Coating	Predicted service life (year)
Epoxy glass-flake paint	3.7
Polyurethane paint	3.8
Cement-based waterproof coating	43
Silane-based water repellent coating	77

Li *et al.* (2015) calculated service lives of some organic coating for concrete from the two types of artificially accelerated aging experiments, as shown in **Table 2-3**. According to their investigation, the service life of silane-based water repellent coating was twice as long as that of cement-based coating, and was almost twenty as long as that of epoxy and polyurethane. However, by studying the long-term water

absorption of silane immersed concrete, some researchers had found that the silane has enough long-term protective effect.

Pan *et al*. (2017b) reported that silane and siloxane could only control the moisture content of the concrete substrate, but they cannot reduce the air permeability. Hence, the diffusivity of CO2 of concrete did not change after the application of silane or siloxane (Basheer, 1997; Suleiman, 2014).

Meier and Wittmann (2011) reported that the types of hydrophobic agent and the concrete substrate influence the penetration depth of the silane-based surface penetrants into the concrete. Concrete surface imperfections, such as bugholes, cracks, pits and craters, may reduce the protective effect of the treatment agents. Bugholes never affect the structural strength of concrete (Yoshitake *et al*., 2018). However, their presence is considered a nuisance since constructors are worried that they may bring insufficient coating applications. Hence, surface finishing and grinding are required before coating (Ozkul and Kucuk, 2011). It should be noted that the additional finishing work causes an increase in construction cost and time.

2.6   SUMMARY AND IMPLICATIONS

The surface bughole on concrete is a potential durability problem, especially in a harsh environment. It may influence the internal and external properties of concrete. c These tunnels located in the cold region are exposed to environmental extremes. Salt scaling in the cold area occurs since the combined F-T cycles and saltwater. It is supposed that the bugholes on concrete surface worsen the F-T resistance of tunnel lining and deteriorate the surface scaling. Besides, surface bughole is also supposed to cause the insufficient application of surface treatment and worsen chloride penetration in the marine environment. However, a few types of research focus on the deterioration resulting from the factor of surface bughole. Hence, the investigation of the effect of bugholes on concrete degradation is needed.

Chapter 3: Quantification of Bugholes and Local Scaling on Concrete Surface by Image Analysis

3.1 GENERAL

This chapter describes the image analysis adopted by this research to achieve the aims and objectives stated in section 1.3 of Chapter 1 that quantitively evaluate the surface scaling on concrete surface.

Section 3.1 compares two evaluation methods for surface scaling, which are the visual inspection and image analysis method, and discusses the research significance.

Section 3.2 and section 3.3 detail the preparation of concrete specimens and presents the test method of the F-T test, respectively.

Section 3.4 presents the test results of the F-T test and discusses the application of image analysis for surface scaling. Section 3.5 proposes a degradation grade scale based on the area-ratio.

Section 3.6 summarizes and concludes the findings in this chapter.

3.1.1 Visual inspection

The grading method based on visual inspection is occasionally used to assess the surface quality of concrete. ACI Committee 116 report (ACI 116R) (ACI Committee 116 and American Concrete Institute 2000, 2000) describes concrete scaling as local flaking or peeling away of the near-surface portion of hardened concrete or mortar. According to the report, "light", "medium", "severe" and "very severe" are defined by the loss of surface mortar down to depths of less than 5 mm, 5-10 mm, 5-10 mm to 10-20 mm around aggregates, and greater than 20 mm, respectively, as shown in **Table 3-1**.

Table 3-1 Visual rating scale of ACI 116R

Rating	Loss of depth
Light	5 mm
Medium	5-10 mm
Severe	5-10 mm to 10-20 mm around aggregates
Very severe	More than 20 mm

ASTM C 672/C 672M (ASTM, 2012) gives the visual rating-scale of surface scaling, as shown in **Table 3-2**. This grading method provides a quick and convenient way to evaluate surface scaling. However, these visual grading methods may be varied by inspectors, and it may cause subjective and inaccurate evaluation. Both the ACI 116R and ASTM 672/C 672M assess surface scaling based on depth. Most local scaling on a concrete surface is caused by the loss of light depth. It may be hard to quantitatively evaluate such local scaling in a general way. Hence, a quantitative evaluation method for local scaling is necessary to assess the deterioration of concrete appropriately.

Table 3-2 Visual rating scale of ASTM C 672/C 672M

Rating	Condition of surface
0	no scaling
1	very slight scaling (3 mm [1/8 in.] depth, max, no coarse aggregate visible)
2	slight to moderate scaling
3	moderate scaling
4	moderate to severe scaling
5	severe scaling (coarse aggregate visible over entire surface)

3.1.2 Image analysis

The colored image analysis Concrete Vision Evaluation (CVE) developed by our lab is based on Red/Green/Blue (RGB) value of color photographs taken by a commercial digital still camera. Each pixel in a color image consisted of the red (R), green (G), and blue (B) color. Therefore, each pixel has a specific RGB value.

The image analysis to detect and evaluate bugholes is described as follows (Yoshitake *et al*., 2018):

1. Import a digital image in the software. Then select a typical bughole in the evaluated photographic image, and the average RGB values of the pixels are determined as reference numbers of red/green/blue.

2. The RGB values of each pixel in the photographic image are compared with the reference number of RGB.

3. When all RGB values of a pixel are low than the reference criteria, the pixel is estimated as an element of the photographic image of the bugholes.

4. When multiple pixels showing a bughole are adjacent to each other, they are combined and estimated as a larger photographic image of the bughole.

5. The dimensions and X-Y coordinates of estimated bugholes are automatically calculated by counting pixels. The reference length is determined by recalculating the pixels of a steel ruler in the evaluated photographic image.

A comparative test conducted by Yoshitake *et al*. (2018) shows that even invisible bugholes (diameter < 1 mm) can be detected in the developed system, whereas such bugholes are hardly detected in the detailed visual survey. Further information on image analysis CVE can be found in the previous papers (Maeda *et al*., 2017; Yoshitake *et al*., 2018).

With the benefits of high accuracy and efficiency, therefore, the image analysis is applicable to detect local scaling deteriorations. This chapter employs the image analysis to quantify the scaling area-ratio to evaluate the local scaling on a concrete/mortar surface.

3.1.3 Research significance

Surface scaling is observed as local flaking of the near-surface portion of mortar. Although visual inspection is a quick and convenient way to evaluate surface scaling, this method is based on the depth of loss and probably cause subjective and inaccurate rating. The image analysis can detect the numbers of bugholes and calculate the bughole area and area-ratio. It emphasizes on the image color of the concrete surface and the scaling, and it can evaluate surface deterioration quantitatively. This chapter conducted an F-T test on mortar specimens having artificial holes and discussed the influence of surface holes due to the local scaling. It confirmed the actual application of the color image analysis method for the quantitative evaluation of surface deterioration. Besides, this chapter gave a degradation grade scale based on deterioration area-ratio.

3.2   PREPARATION OF CONCRETE SPECIMENS

3.2.1 Materials and mixture proportion

Mortar materials used in this chapter were sea sand (density: 2.58 g/cm^3) and ordinary Portland cement (density: 3.16 g/cm^3) defined in the Japan Industrial Standard (JIS R 5210). Water-cementitious material ratio and cement/sand mass ratio of mortar were 0.45, 0.5 (1:2), respectively. The mortar had a compressive strength of 45 MPa at the age of 28 days.

3.2.2 Test specimens

To make surface holes, the mortar was cast in a steel mold (150 mm × 150 mm × 60 mm) with wood plates at the bottom having various sizes of round screws, as shown in **Figure 3-1**. Every three of specimens with the same hole size, including hole diameter of 2 mm, 4.5 mm, 6.9 mm, 9.4 mm, 14 mm, and no holes, as given in **Table 3-3**. **Figure 3-2** shows the specimens demolded at the age of 1 day. After that, mortar specimens were covered with aluminum tape as a dike along the perimeter of testing surfaces, as shown in **Figure 3-3**. In addition, an adhesive was employed to bond aluminum tape to the surface.

Table 3-3 Hole size of specimens

Specimen	Hole size (mm)	
	Diameter	Depth
1		
2	-	-
3		
4		
5	2	0.5
6		
7		
8	4.5	1.2
9		
10		
11	6.9	1.9
12		
13		
14	9.4	2.5
15		
16		
17	14	3.7
18		

Figure 3-1 Steel mold with wood plates having various sizes of round screws

No artificial hole   2 mm   4.5 mm   6.9 mm   9.4 mm   14 mm
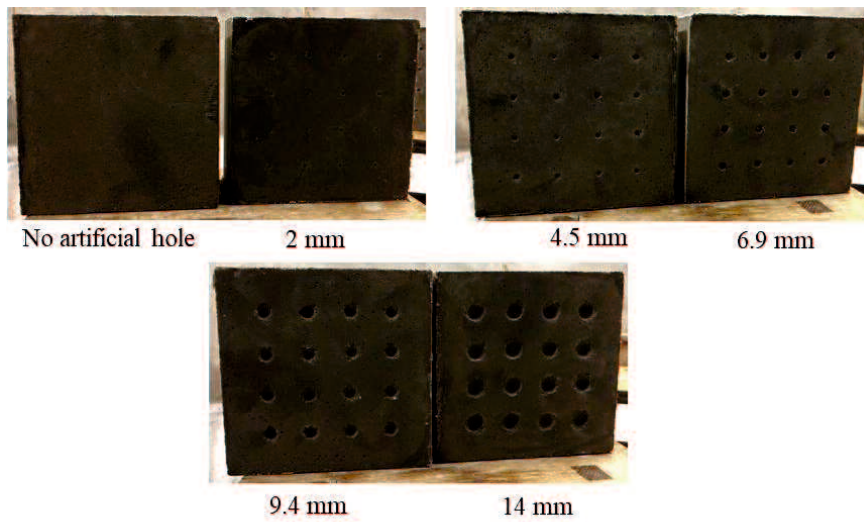
Figure 3-2 Surfaces of mortar specimens with holes in various diameters

Aluminum tape

4% calcium chloride solution

6

60

50

150

150

(mm)
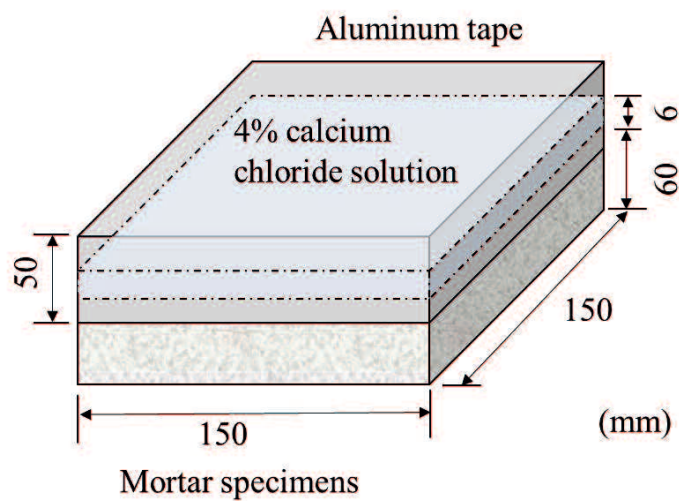
Mortar specimens

Figure 3-3 Mortar specimen in the F-T test
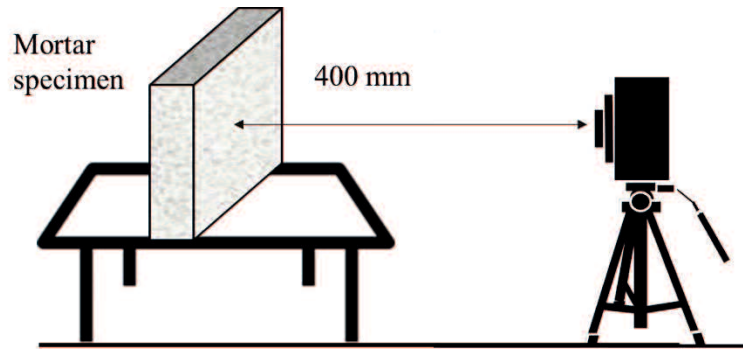
Figure 3-4 Photographic test condition

3.3 FREEZE-THAW TEST

All specimens were subjected to 100 F-T cycles. In the F-T test, mortar specimens retained 4 % calcium chloride water of 6 mm depth and were placed in a cooling chamber. The freezing temperature was -15 °C for 16 hours, while thawing was performed in a natural ventilation condition for 8 hours. A digital camera recorded the surface conditions with a shooting distance of 400 mm, as shown in **Figure 3-4**.

3.4 TEST RESULTS AND DISCUSSION

After the F-T test, surface scaling was evaluated by both visual inspection methods and the image analysis method.

3.4.1 Surface scaling evaluated by visual inspection

Table 3-4 gives the rating grade by the visual inspections. Based on the ACI criterion, all mortar specimens indicated "light scaling" since the loss of surface mortar down to depths is less than 5 mm. Moreover, based on the visual rating scale of ASTM C 672/C 672M, all mortar specimens were rated as level 1 because scaling depths were lower than 3 mm. These visual evaluation methods evaluate the local scaling in a general way and ignore the deterioration area.

3.4.2 Surface scaling evaluated by image analysis

Deterioration area-ratio
The deterioration area-ratio r_d is defined as

$$r_d = \frac{s_d}{s}$$ **Equation 3-1**

where S_d is the total area of pixels estimated as holes and scaling, and S is the evaluation area of a graphical image used in the image analysis.

Table 3-4 Visual evaluation by ACI 116R and ASTM C 672/C 672M

Specimen	ACI 116R	ASTM C 672/C 672M
1	light	1
2	light	1
3	light	1
4	light	1
5	light	1
6	light	1
7	light	1
8	light	1
9	light	1
10	light	1
11	light	1
12	light	1
13	light	1
14	light	1
15	light	1
16	light	1
17	light	1
18	light	1

The deterioration area-ratios of test surfaces before and after 100 F-T cycles (r_{d0} and r_{d100}) were performed by the image analysis, and their relationship is shown in **Figure 3-5**. Specimen 1-2, 4-6, 7-9, and 10-11, having the same size of surface holes, respectively, showed less deterioration during the F-T cycles. The observation implies that the degradation of the surface with small holes can be negligible.

Scaling area-ratio

Scaling area-ratio r_s occurring in the 100 F-T cycles is calculated as follows:

$$r_s = r_{d100} - r_{d0}$$ **Equation 3-2**

Figure 3-6 shows the relation of initial deterioration area-ratio r_{d0} and scaling area-ratio r_s. Specimens 1 and 3-11 indicated slight scaling. On the other hand, Specimen 14-15 and 17-18 had severe scaling around their larger surface-holes. The observations confirm the former F-T test result of concrete. It meant that the local scaling main occurred at the edge of bugholes, where were subjected to multi-directional frost damages, while the surface having fewer bugholes showed hardly

local-scaling. Therefore, it can be concluded that the local scaling is affected by surface bugholes. The initial surface quality problems, such as surface bugholes and spalling, are possible to increase the permeability of concrete and to accelerate the penetration of chloride ion.
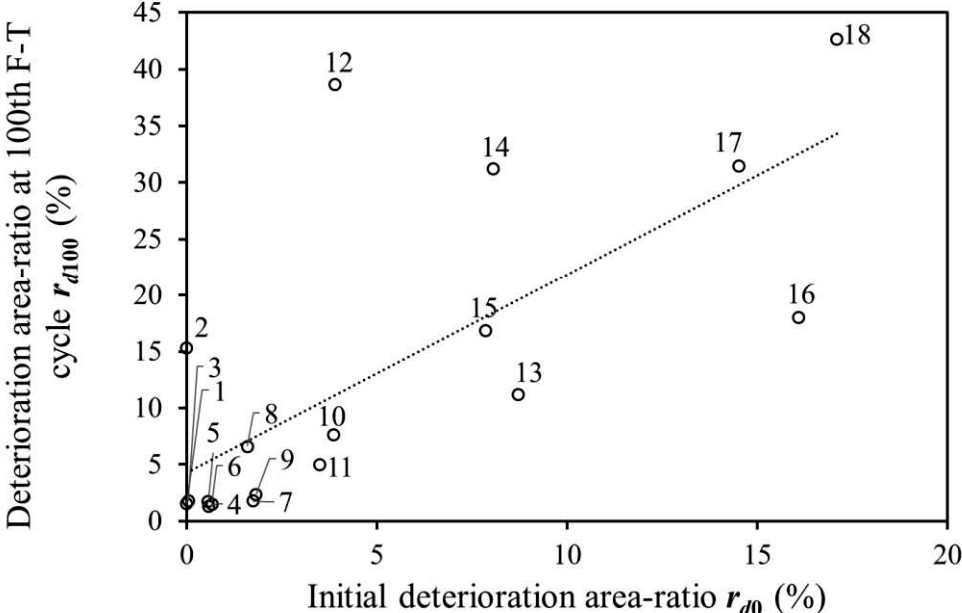
Figure 3-5 Relation of deterioration area-ratio before and after 100 F-T cycles
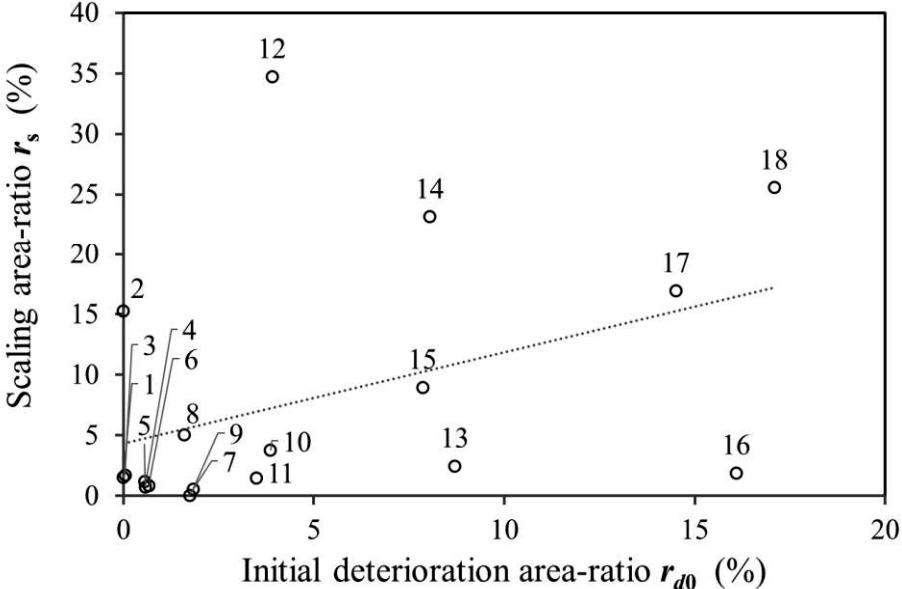
Figure 3-6 Relation of initial deterioration area-ratio r_{d0} and scaling area-ratio r_s in 100 F-T cycles

3.5 DEGRADATION GRADE SCALE BASED ON THE AREA-RATIO

To evaluate surface deterioration precisely, the present study proposes a grading scale based on the area-ratio given in **Table 3-5**.

Table 3-5 Degradation grade scale based on deterioration area-ratio r_d

Grade	r_d	Surface condition
0	$\leq 0.01\%$	no deterioration
1	$\leq 1\%$	very slight deterioration
2	$\leq 5\%$	slight to moderate deterioration
3	$\leq 10\%$	moderate
4	$\leq 20\%$	moderate to severe deterioration
5	$>20\%$	severe deterioration

For grade 0, deterioration area-ratio under 0.01% is acceptable, while the image analysis can detect invisible bugholes and holes caused by the scaling (< 1 mm). The degradation is not significant for the evaluation of the surface quality. The grades 1-4 refer to the hole area-ratio of Specimen 4-6, 7-12, 13-15, 16-18, respectively. For severe deterioration grade 5, scaling area-ratio is over 20%.

According to the degradation grade scale, the tested mortar specimens were rated in **Table 3-6**. It assesses the degradation of specimens concisely and precisely based on the area-ratio. This grading scale is a complement with visual inspection methods by scaling depth though further investigation is needed to validate the application of the proposed deterioration grade scale.

Figure 3-7 shows the processed image of Specimen 18 before and after the F-T test. The scaling, occurring around holes in a slight depth, was detected by the image analysis. It is confirmed that the image analysis is applicable to quantify surface deteriorations.
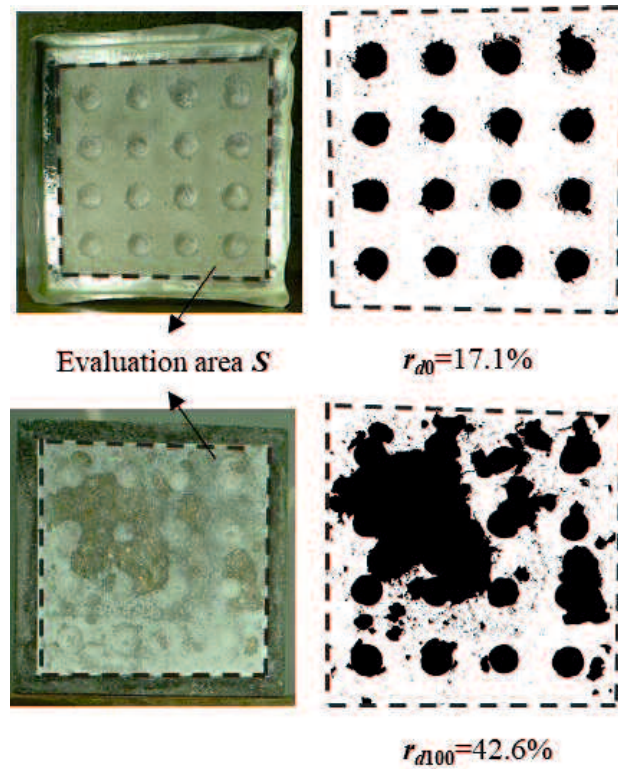
Figure 3-7 Processed images of specimen 18 by image analysis before and after 100 F-T cycles

Table 3-6 Deterioration grade of mortar specimens

Specimen	Before F-T test		100th F-T cycle	
	r_{d0}	Grade	r_{d100}	Grade
1	0	0	1.6	2
2	0	0	15.3	4
3	0	0	1.8	2
4	0.6	1	1.3	2
5	0.6	1	1.8	2
6	0.7	1	1.5	2
7	1.7	2	1.8	2
8	1.6	2	6.6	3
9	1.8	2	2.4	2
10	3.9	2	7.6	3
11	3.5	2	5	2
12	3.9	2	38.6	5
13	8.7	3	11.2	4
14	8.1	3	31.2	5
15	7.9	3	16.8	4
16	16.1	4	18	4
17	14.5	4	31.5	5
18	17.1	4	42.6	5

3.6 SUMMARY AND CONCLUSIONS

This chapter presented the application of image analysis for detecting surface deterioration, including surface bugholes and surface scaling. The image analysis is useful for detecting the surface scaling, and a deterioration scale based on the deterioration area-ratio was proposed. The conclusions of this chapter are summarized as follows.

(1) The image analysis provided a quantitative evaluation method for local scaling of concrete surface. It was applicable for the deterioration detection, including invisible surface scaling under the F-T cycles.

(2) The local scaling was affected by initial surface holes or bugholes before the F-T test.

(3) The proposed grading-scale based on the area-ratio was useful for the evaluation of surface deterioration.

The image analysis in this chapter can quantify surface deterioration by using the two-dimensional area. It can be a complement to the conventional visual inspection methods by scaling depth. Further research and practical application study are needed to validate the proposed scale.

Chapter 4: Effect of Bugholes on Freeze-Thaw Durability of Tunnel Lining Concrete

4.1 GENERAL

Salt scaling on a concrete surface with bugholes is critical because bugholes are exposed to frost attack from various directions and reduce the permeability properties of concrete. Lining concrete of a road tunnel at portals is occasionally exposed to F-T cycles and de-icer solutions by traffic cars. Hence, salt exposure and superficial damage should be considered for a realistic scenario of road tunnels. The foci of this chapter are to examine the effect of surface bugholes on the frost durability of tunnel lining sidewalls and to evaluate the degradation of the vertical concrete surface quantitatively by using the image analysis.

This chapter presents the synergetic and negative effects of bugholes on the local scaling of tunnel lining concrete exposed to F-T cycles. A laboratory F-T test of 300 cycles was conducted to examine the frost deterioration of tunnel lining concrete. Test parameters included air entrainment agent and surface bughole area-ratio (r_b), which is defined as the ratio between the bughole area and the total evaluated concrete surface area.

Section 4.2 presents the preparation of concrete specimens, and section 4.3 describes the F-T test.

Section 4.4 introduces the image analysis that is used to detect surface deteriorations.

Section 4.5 gives the test results and discusses the types of surface deteriorations, deterioration of bughole, and chloride penetration.

Section 4.6 summarizes and concludes the findings in this chapter.

4.2   PREPARATION OF CONCRETE SPECIMENS

4.2.1 Materials and mixture proportions

Lining concrete of NATM tunnels is generally constructed using cast-in-place concrete and arch-shaped form (called as "center"). The study focused on the effect of bugholes, which often appear on the sidewall of tunnel lining, on the F-T durability. Concrete materials used in this chapter are given in **Table 4-1**. All concrete specimens were made with ordinary Portland cement defined in the Japan Industrial Standard (JIS R 5210). Although most tunnel lining at portals is constructed using reinforced concrete (RC), generally, tunnel lining concrete is plain concrete without steel-reinforcement. A coarse aggregate of 40 mm (max.) is often used in plain concrete, such as tunnel lining, so the present study employed the aggregate of 40 mm.

<div align="center">Table 4-1 Materials of concrete</div>

Types	Symbol	Materials	Density (g/cm^3)
Cement	OPC	Ordinary Portland cement [a]	3.16
Fine aggregate	S1	Sea sand	2.60
	S2	Limestone sand	2.69
	S3	Crushed sand	2.58
	S4	Limestone sand	2.60
Coarse aggregate	G1	Crushed sandstone Max.-Min. size: 40–20 mm	2.72
	G2	Crushed sandstone Max.-Min. size: 20–10 mm	2.73
	G3	Crushed sandstone Max.-Min. size: 15–5 mm	2.70
	G4	Crushed sandstone Max.-Min. size: 15–5 mm	2.73
Admixture	WRA	Water reducing agent	1.0
	AE	Air entraining agent	1.0
	AE-WRA	Air entraining and water reducing agent	1.0

[a]Japan Industrial Standard (JIS). Portland cement, JIS R 5210.

Table 4-2 The mixture proportion and properties of concrete

Specimens	No.1	No.2	No.3	No.4	No.5	No.6
Concrete type	LM [a]	RM [b]	LM [a]	LM [a]	LM [a]	LM [a]
Water-cement ratio (*w/cm*)	0.59	0.59	0.59	0.59	0.59	0.59
Water (kg/m^3)	165	172	165	165	165	165
Cement (kg/m^3)						
OPC	280	292	280	280	280	280
Fine aggregate (kg/m^3)						
S1	756	-	366	366	366	366
S2	-	264	366	366	366	366
S3	-	264	-	-	-	-
S4	-	352	-	-	-	-
Coarse aggregate (kg/m^3)						
G1	455	-	454	454	454	454
G2	342	581	341	341	341	341
G3	342	-	341	341	341	341
G4	-	387	-	-	-	-
WRA (kg/m^3)	0.42	-	2.8	2.8	2.8	2.8
AE (kg/m^3)	0.021	-	-	-	-	-
AE-WRA	-	2.92	-	-	-	-
Air (%)	5.0	5.5	-	3.8	2.8	3.9
Slump (cm)	8.5	16.5	17.0	17.0	14.5	17.5
f_{cy} (MPa)	30.8	34.4	22.4	21.7	25.5	21.4
Form angle	30°	30°	0°	15°	30°	45°
Evaluation area on surface	1F/1R [c]	2F/2R [c]	3F/3R [c]	4F [c]	5F [c]	6F/6R [c]

[a] Concrete mixed in the laboratory.

[b] Ready-mixed concrete.

[c] F: evaluated front surface; R: evaluated rear surface.

The mixture proportions are given in **Table 4-2**. The water-cementitious material ratio (w/cm) of the tested concrete was 0.59, which was decided by referring to a concrete mixture used in general tunnel lining. The proportions were designed by referring to conventional lining concrete having a slump of 15 cm and specified compression strength of 21 MPa at 28 days. It should be noted that the concrete for specimen No.2 was made in a ready-mixed concrete to examine the effects of bugholes in practical tunnel concrete while other concrete specimens were produced in the laboratory. The concretes tested in the study are classified into a low-strength concrete, so it might indicate lower resistance to F-T cycles than the mid- / high- strength concrete.

4.2.2 Test specimens

The F-T test used six concrete specimens since the limited space in the freezing chamber. Specimens were cast in a steel form, which simulates the tunnel lining concrete constructed by NATM, as shown in **Figure 4-1** (a). Specimens have a dimension of 300 mm × 300 mm × 750 mm, and the negative angle (α in **Figure 4-1** (b)) of steel form can vary from 0º to 45º. The front and rear surface of specimens are illustrated in **Figure 4-1** (b). The six concrete specimens were cast at a different angle each, in the steel form, as shown in **Table 4-2**. The specimens No.1 and 2 were cast at 30º angle of steel form, while the specimens No.3-6 were cast at the angles 0º, 15º, 30º, 45º of steel form, respectively.

Each concrete specimen was consolidated using a vibrator placed in the middle of the specimen for 60 s. The vibrator had a diameter of 28 mm and a frequency of 220-280 Hz. During vibration, air and water bubbles at the rear surface arise and escape easily. On the other hand, such bubbles on the front surface hardly move even under the consolidating vibration. Therefore, the rear surface has fewer bugholes than the front surface. The steel form was removed after 48 h, and concrete specimens were cured at the atmospheric conditions.

(a) dimension of steel form
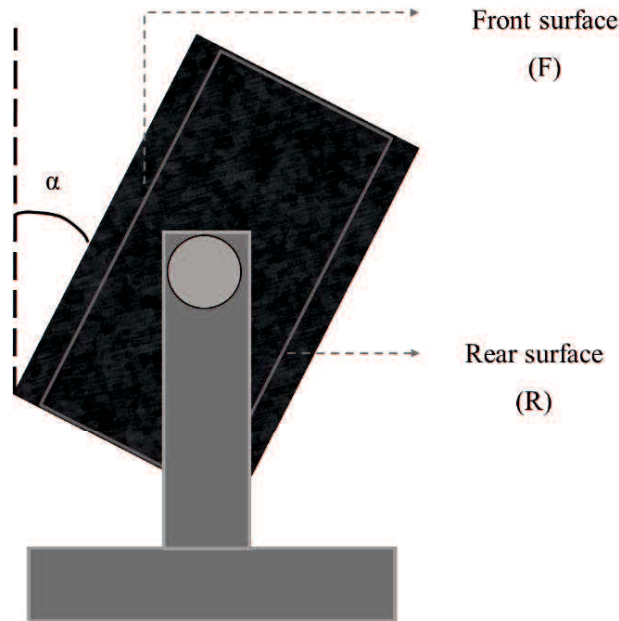
(b) front surface and rear surface of specimen and the negative α-angle of form

Figure 4-1 Steel form simulating tunnel lining constructed by NATM

4.3 TEST METHOD

All test specimens were subjected to 300 F-T cycles. The calcium chloride solution was sprayed on the vertical concrete surface (300 mm × 750 mm) to avoid the saturated condition and obtain surface scaling on concrete. It is noted that calcium chloride is commonly used as a deicer in western Japan. The 7% chloride solution was sprayed on the concrete surface at 400 g/m2 in accordance with the usage by the manufacturer. The evaluation surfaces are given in **Table 4-2**. The rear surfaces of the specimens No.4 and 5 were not tested. Left and right surfaces and the upper surface were covered with plastic sheets to avoid the impact of salt-water during the F-T test. The tested concrete specimens were placed in a freezing chamber (2.5 m × 1.6 m) to simulate the sidewall of tunnel lining under cold temperature, as shown in **Figure 4-2**. The freezing temperature was -15 °C for 16 hours, and thawing was performed at natural ventilation conditions for 8 hours. **Figure 4-3** shows the position of the specimens in the freezing chamber.

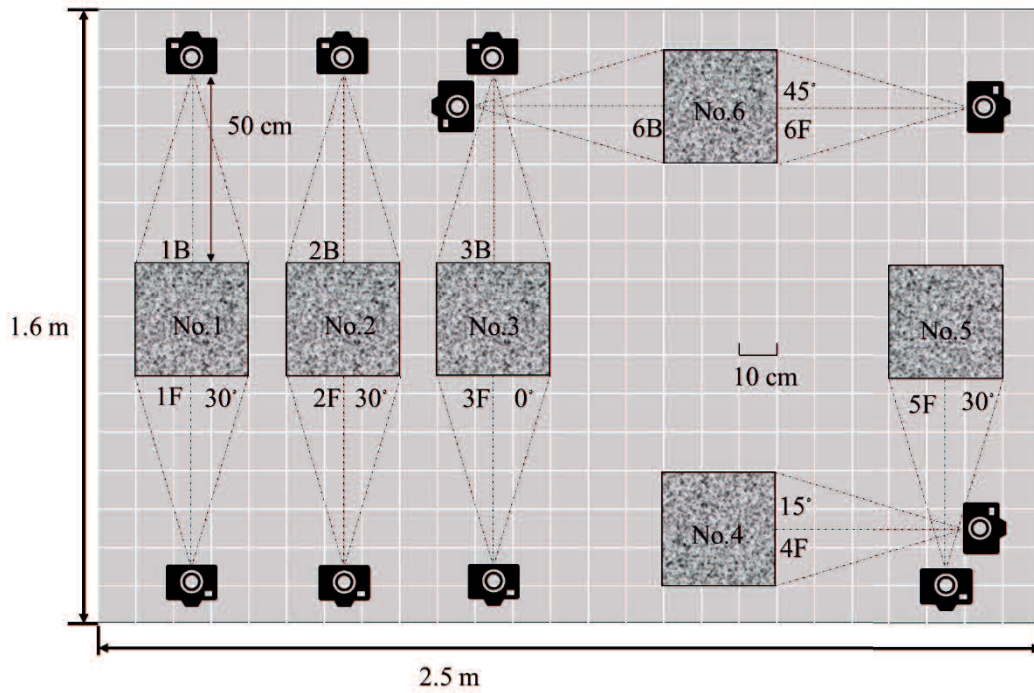**Figure 4-2** Specimens in the freezing chamber

Figure 4-3 Position of concrete specimens in cooling chamber

Influence of Surface Bugholes on Freeze-Thaw Degradation of Tunnel Lining Concrete

After 240 F-T cycles, to examine the effect of horizontal position on frost durability, the concrete specimens No.1, 2, 4, 5, and 6 were horizontally laid on the floor such that the front surfaces faced upside and the front surfaces were evaluated, while the chloride solution was sprayed on the front surfaces in each cycle. **Figure 4-4** shows a schematic of the vertical and horizontal positions of specimens in the test. Specimen No.3 was vertically erected, and the chloride solution was sprayed on both front and rear surfaces.
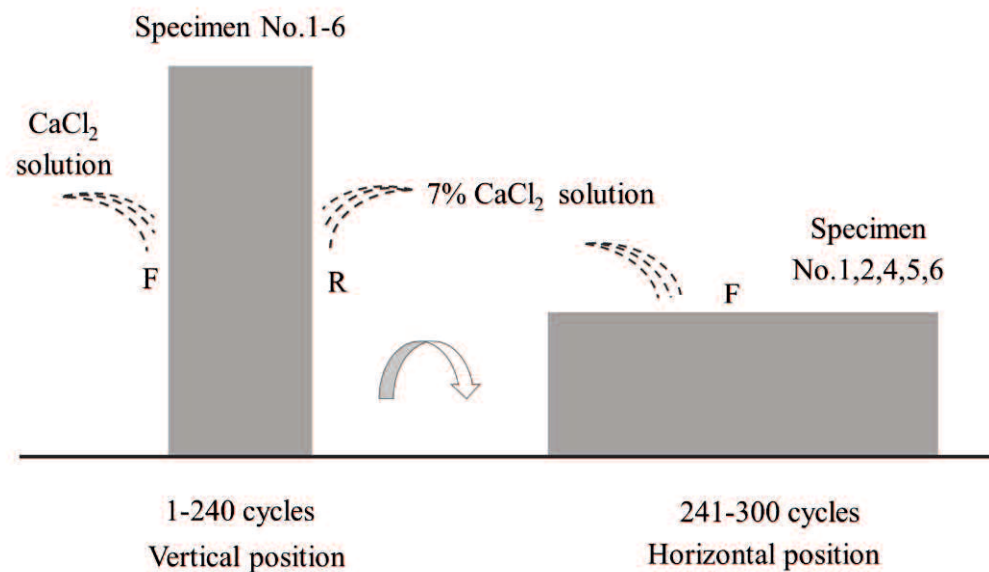
Figure 4-4 Vertical and horizontal positions of specimens in F-T test

4.4 DETERIORATION DETECTED BY IMAGE ANALYSIS

Owing to the huge size of specimens, the weight loss or internal damage is hard to detect. This study used an image analysis system, Concrete Vision Evaluation (CVE), to detect surface bugholes and observe the deterioration occurring during the F-T cycle test. This system uses digital colored photographs, and based on the RGB value of each pixel, calculates the area of each individual bughole by pixel count. Further information on the CVE image analysis method can be found in Chapter 3 and previous reports (Maeda *et al*., 2017; Yoshitake *et al*., 2018).

The quality of the photographs significantly influences the accuracy of the image analysis. **Figure 4-5** (a)-(b) shows the schematics of the photographic method and the evaluated area of the concrete surface, which was 300 mm × 300 mm on the front and

rear surface. The image analysis used high-quality photographs shot by the same digital still camera under a constant test condition. The shooting distance was 500 mm.
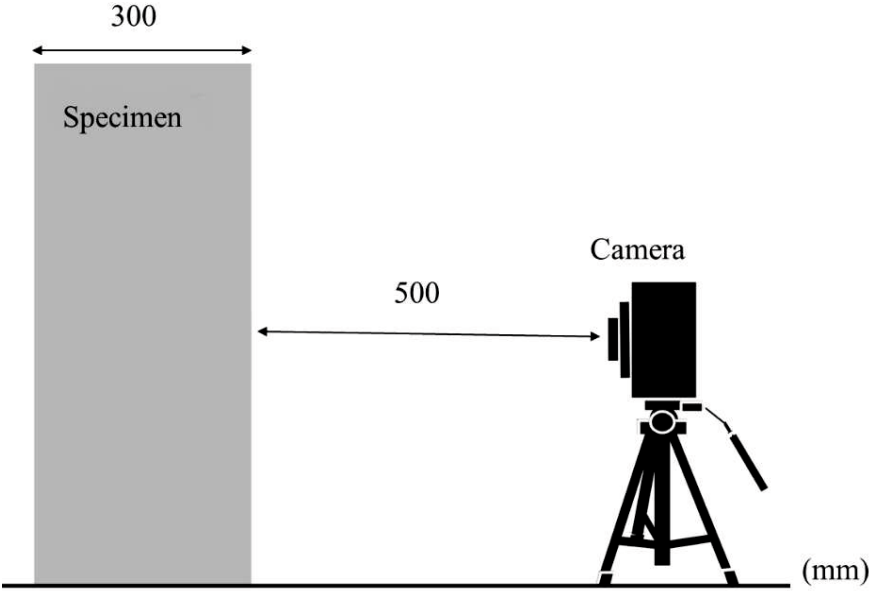
(a) schematics of the photographic method
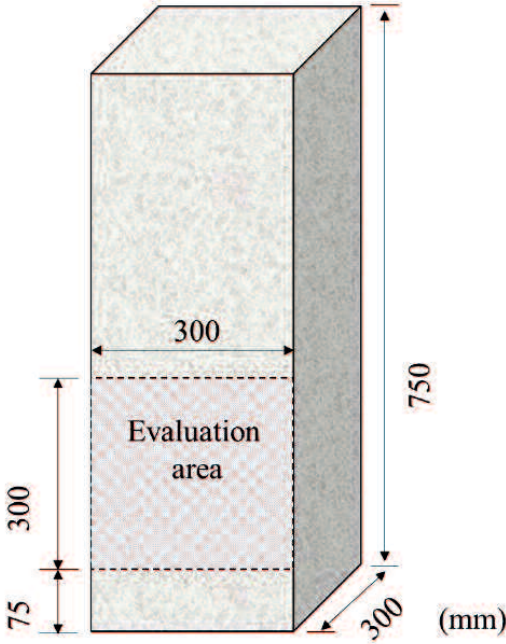
(b) evaluation area of 300 mm × 300 mm of the concrete surface

Figure 4-5 Evaluation method

4.5   TEST RESULTS AND DISCUSSION

4.5.1 Types of surface deteriorations

Concrete surfaces were photographed during F-T cycles, and four types of surface deterioration were observed: (1) deterioration at concrete corner, (2) bugholes' mergence, (3) enlarged bugholes, and (4) pits and craters on the concrete surface. Note is that the deteriorations were caused by the combined effect of F-T cycles and frost attack.

Deterioration at the concrete corner

Severe scaling occurred instantaneously at the corner of concrete specimens because of the multi-directional frost attack.

Figure 4-6 (a)-(b) shows the frost damage at the right corner of the surface 4F from 0 to 300 F-T cycles. Any relation between the concrete deterioration and the presence of surface bugholes was not observed. The main goal of this chapter was to evaluate the effect of surface bugholes. Therefore, the deterioration of the concrete edge was not analyzed in the evaluation.
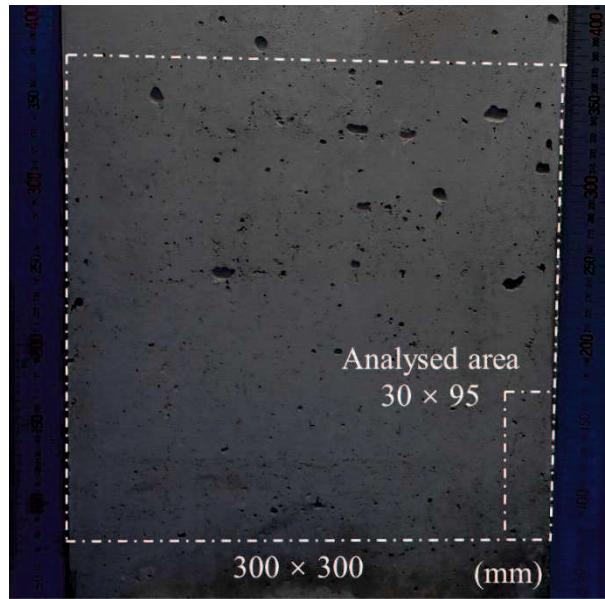
(a) position of scaling damage

0 cycle 61 cycles 100 cycles 150 cycles 200 cycles 300 cycles
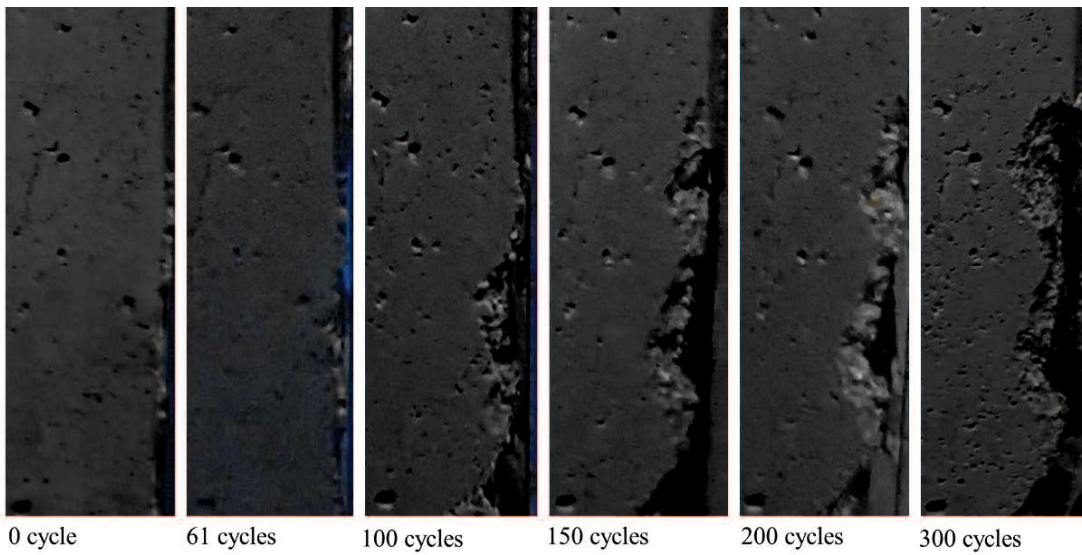
(b) frost damage from 0 to 300 cycles

Figure 4-6 Scaling at the right corner of the surface 4F

Bugholes-mergence

Figure 4-7 shows the merging process of bugholes 1 and 2 on surface 1F. After 60 F-T cycles, bugholes that were initially in proximity to each other merged into newly formed larger holes. The cover-concrete in proximity to bugholes was damaged by frost attack. The bughole-mergence occurred both in visible and invisible bugholes. The mergence of invisible bugholes resulted in larger and more visible holes, as well as pits and craters.
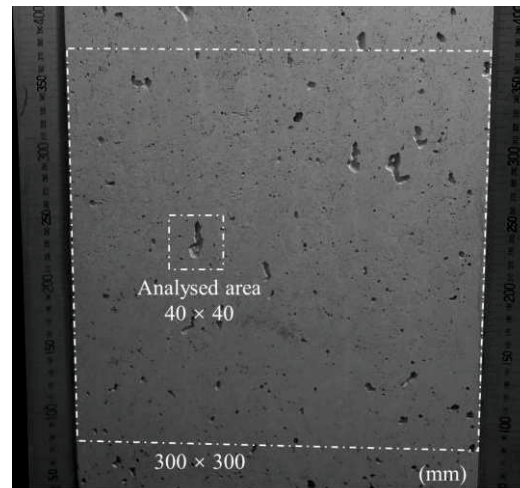
(a) position of deterioration
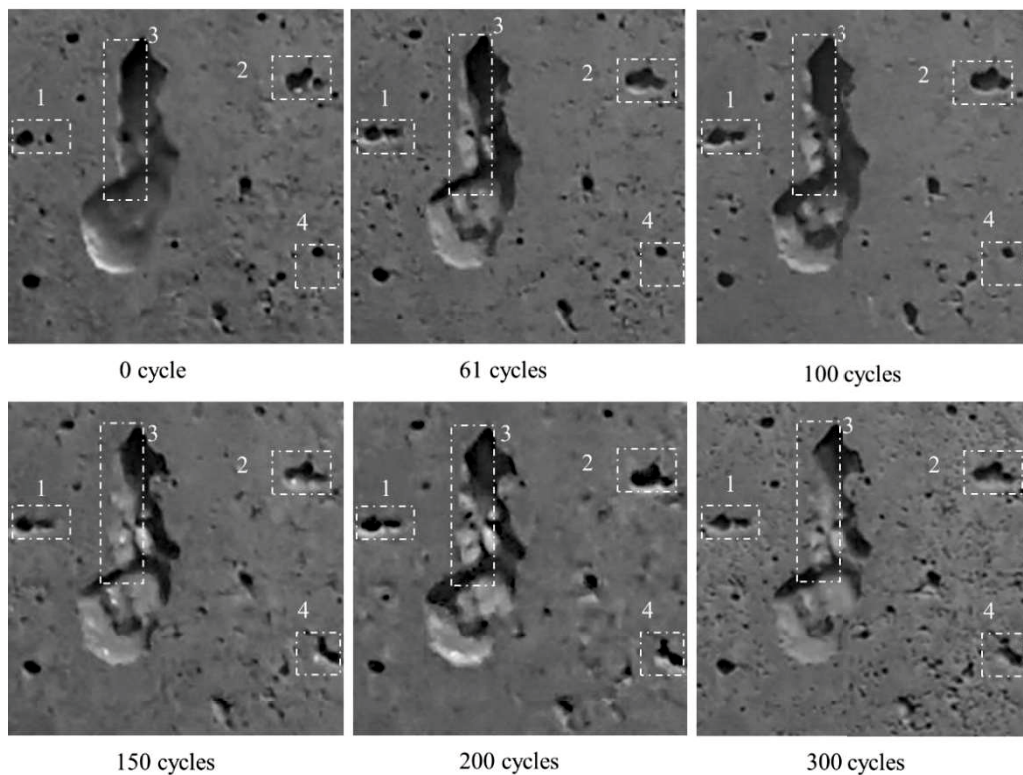
(b) surface holes mergence 1, 2, and enlargement 3, 4 from 0 to 300 cycles

Figure 4-7 Typical local scaling on the surface 1F

Enlargement of bugholes

Single bugholes enlarged due to the frost damage on the edges. Generally, a bughole has both acute and obtuse angles at the flattening surface (**Figure 4-8** (a)). If a surface bughole can be clearly seen in its whole size, the interior surface and the normal concrete surface are characterized by obtuse angles β_2 and β_3, as shown in **Figure 4-8** (b). On the contrary, when a surface bughole does not show its maximum cross-section, the angle between the concrete outer surface and the bughole is usually an acute angle, γ_2 and γ_3, as shown in **Figure 4-8** (c). Compared with the obtuse-angle edges, cover-concrete of acute-angle edges are more susceptible to flaking. **Figure 4-9** (a) and (b) illustrates the enlargement of a bughole on surface 4F, the area of which, at 300 F-T cycles, is three times that of the initial area. In addition, **Figure 4-7** (b) shows the enlargement of surface air-voids 3 and 4. The results show that invisible bugholes enlarged to visible holes. It is of interest that the enlargement and mergence of bugholes happen simultaneously.

| (a) obtuse angle β_1 and acute angle γ_1 | (b) obtuse angle β_2 and β_3 | (c) acute angle γ_2 and γ_3 |
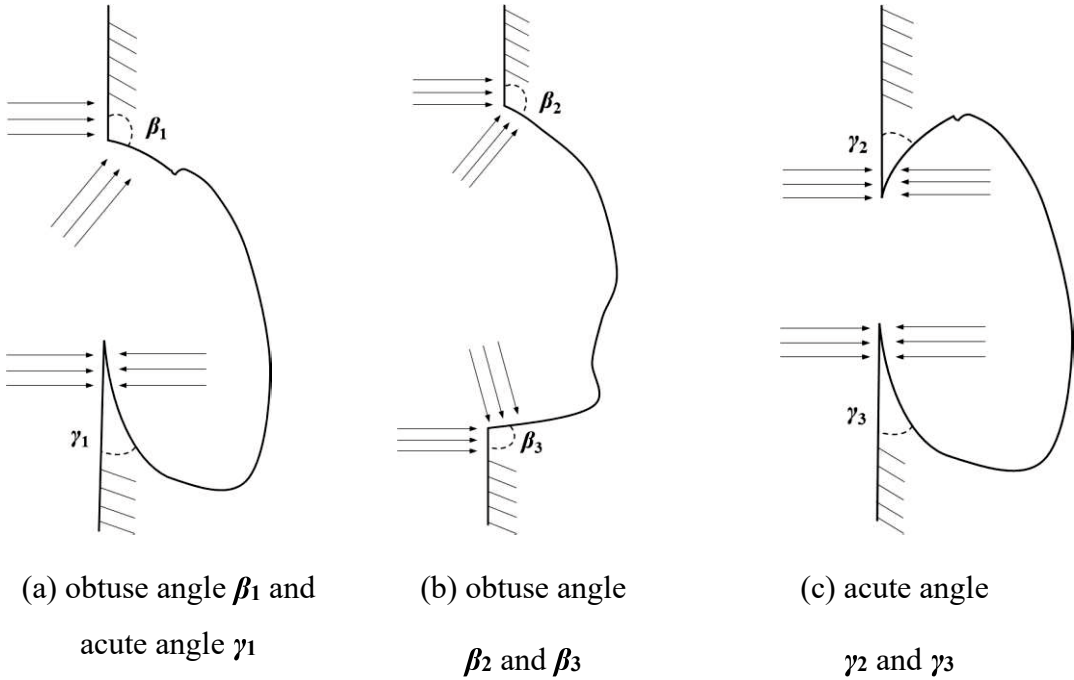
Figure 4-8 The angle between bughole interior surface and flat surface
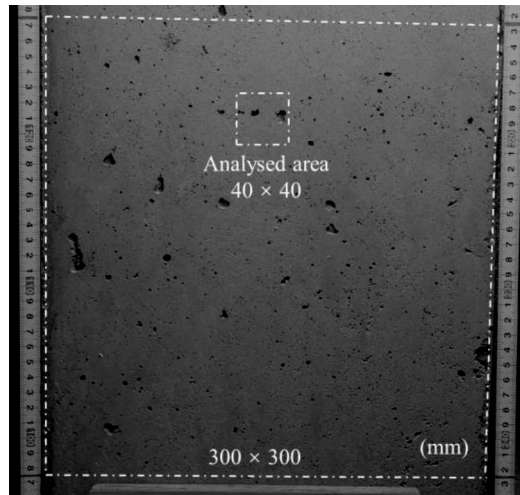
(a) position of analyzed area
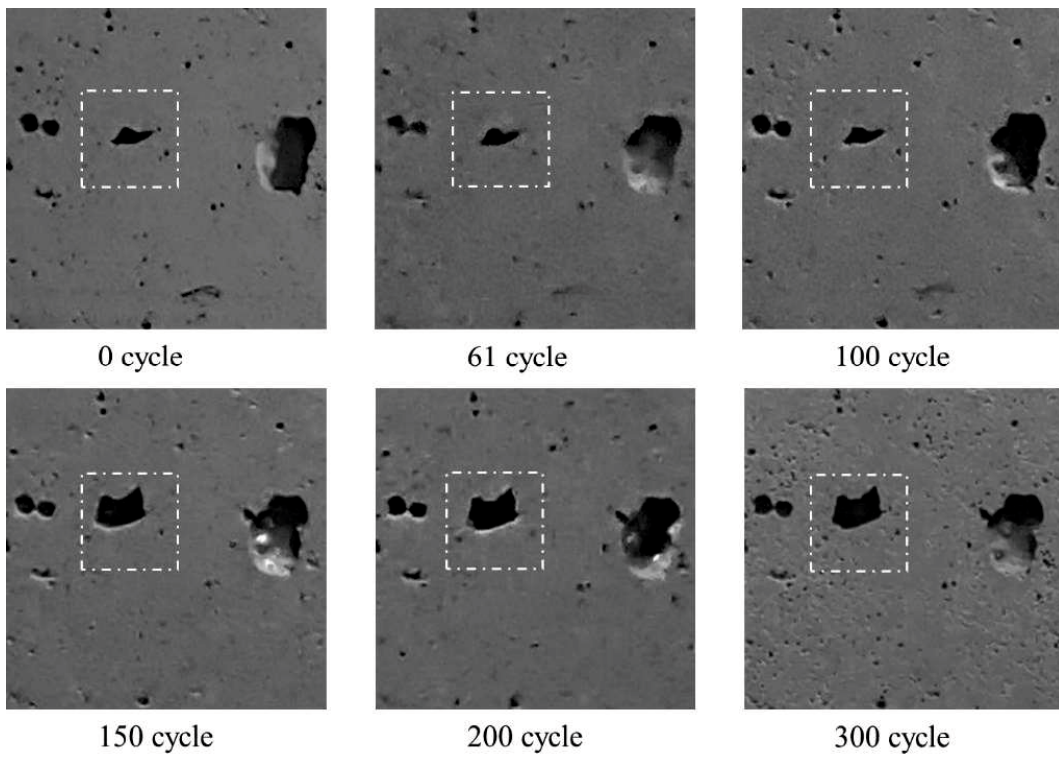
(b) enlargement of the hole from 0 to 300 cycles
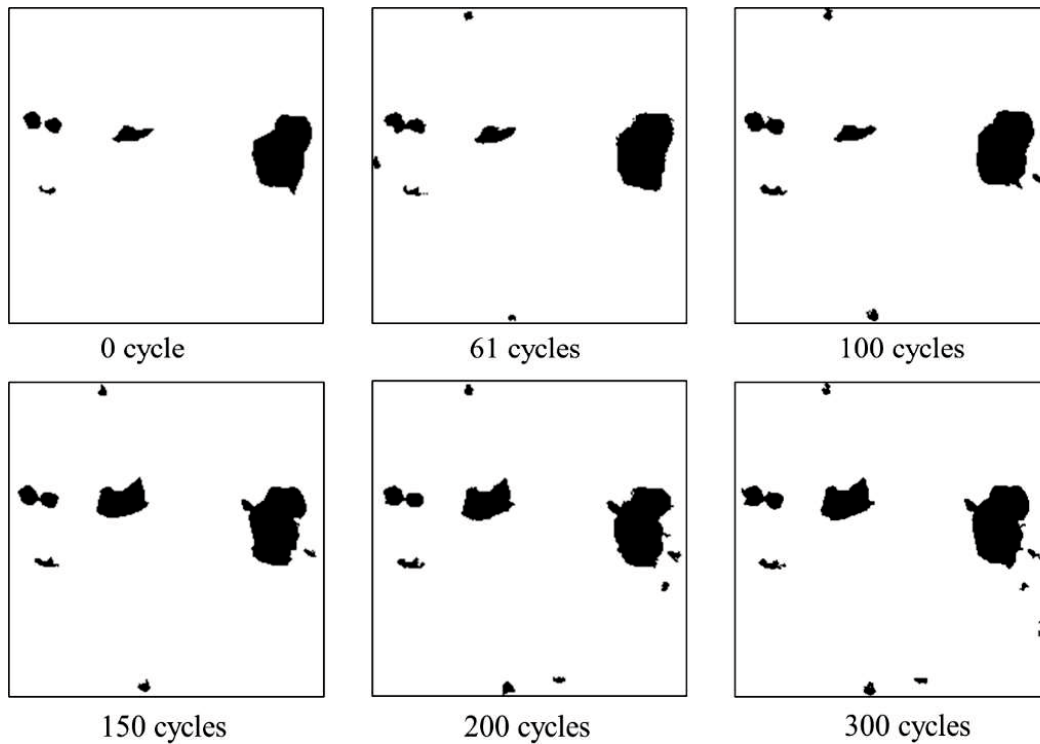
(c) image analysis results (dia. > 1 mm)

Figure 4-9 Enlargement of a hole on surface 3R

Pits and craters on the concrete surface

Figure 4-10 (a) and (b) show the process of porosity formation on surface 6F. The concrete surface subjected to F-T cycles often produces pits and craters, due to mergence and enlargement of invisible bugholes. As the number of cycles increases, the concrete surface gradually becomes more porous, increasing the superficial area. The pits and craters on the concrete surface, together with visible holes, were detected with the image analysis.
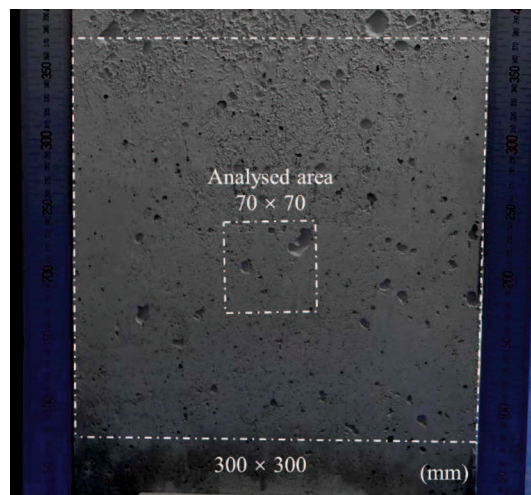
(a) position of analyzed area
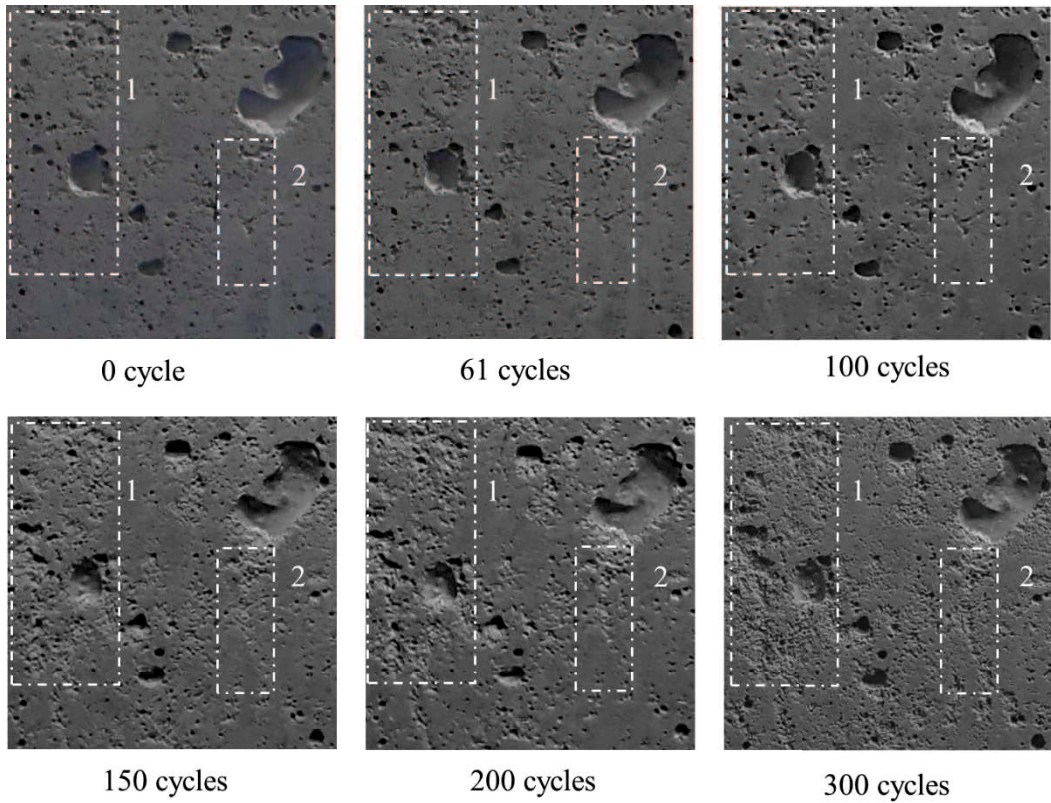
(b) pits and craters from 0 to 300 cycles (1 and 2)

0 cycle
(Dia. > 0 mm)

300 cycles
(Dia. > 0 mm)

0 cycle
(Dia. > 1 mm)

300 cycles
(Dia. > 1 mm)
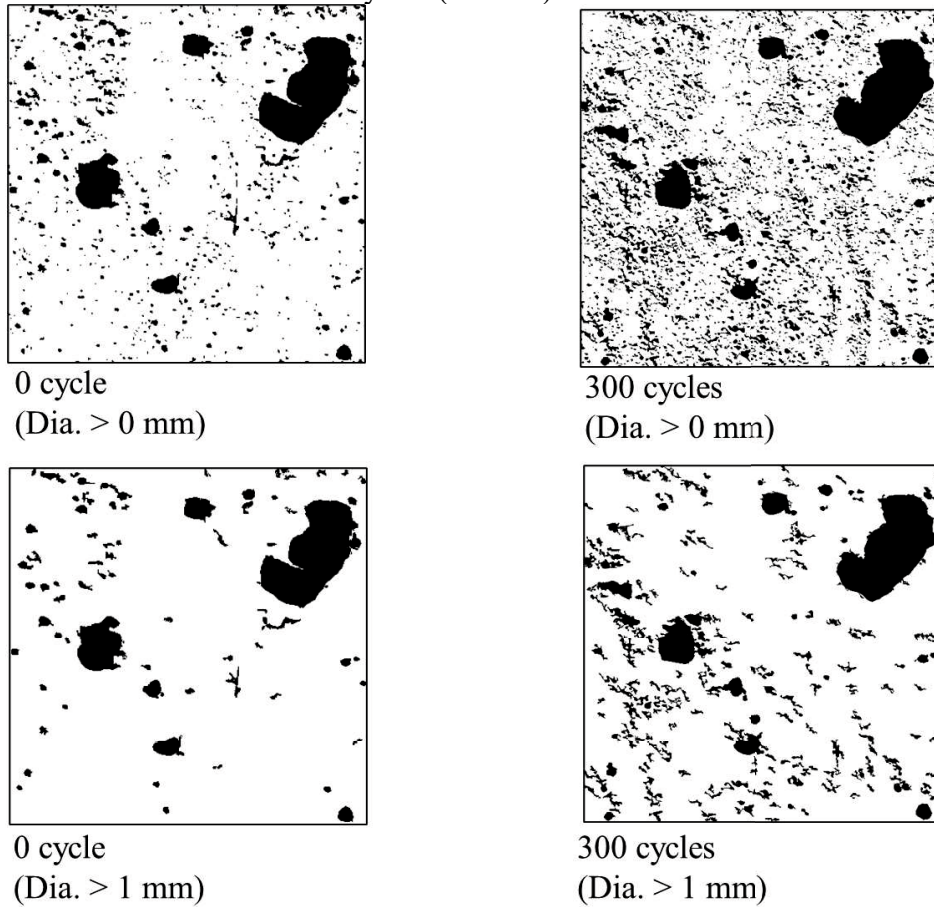
(c) image analysis results

Figure 4-10 Pits and craters on surface 6F

4.5.2 Deterioration of bugholes

Although the deterioration was revealed in the visual inspection, the image analysis developed in the previous study (Yoshitake *et al.*, 2018) was performed to quantify the deterioration area more accurately. We found that the color-tone of the concrete surface is affected by direct / reflected light. Thus, the color-tone of the photographs at different F-T cycles is different due to the presence of water on the concrete surface, causing reflection. Besides, the color-tone of photographs is influenced by shutter speed, aperture, and ISO constant (the sensitivity of a camera sensor to light). The scaling of edge flakes allows more light to reach the hole and highlight the edged area. However, the image analysis can still detect bugholes from a normal surface. The typical surface deteriorations (nominal diameter > 1 mm) were evaluated in image analysis, as shown in **Figure 4-9** (c). It shows that the colored image analysis is a practical technique to quantify the deterioration area, including surface bugholes and scaling. **Figure 4-10** (c) shows the total deterioration area from the image analysis depends on the hole diameter threshold. When increasing this threshold from 0 to 1 mm, the deterioration is clearer. The invisible holes (< 1 mm) are profoundly affected by color-tone and quality of photographs, and they are not a very significant impact on conclusions in image analysis. Therefore, surface holes of a nominal diameter of 1 mm (area 0.79 mm2) or larger were detected and evaluated in this chapter.

The area-ratio of the concrete bugholes was related to the form inclination angle (α-angle). **Figure 4-11**shows that the area-ratio of bugholes (r_b) on the front surface significantly increased in accordance with the α-angle, especially 30° or higher.

Surface deterioration area-ratio (r_N) at N cycle(s) of F-T, quantified by using the image analysis method, is as follows:

$$r_N = r_{sN} + r_b \qquad \textbf{Equation 4-1}$$

where r_{sN} is the scaling area-ratio on the concrete surface. **Figure 4-12** shows that the deterioration area-ratios of the concrete surface slightly increased with F-T cycles.
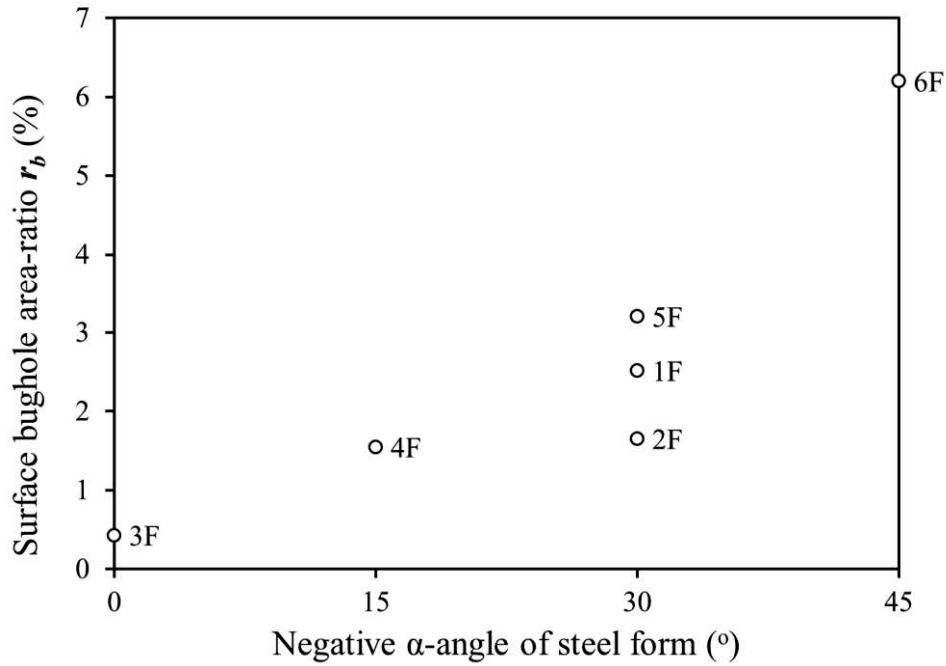
Figure 4-11 Bughole area-ratio r_b of front surface and negative α-angle of steel form
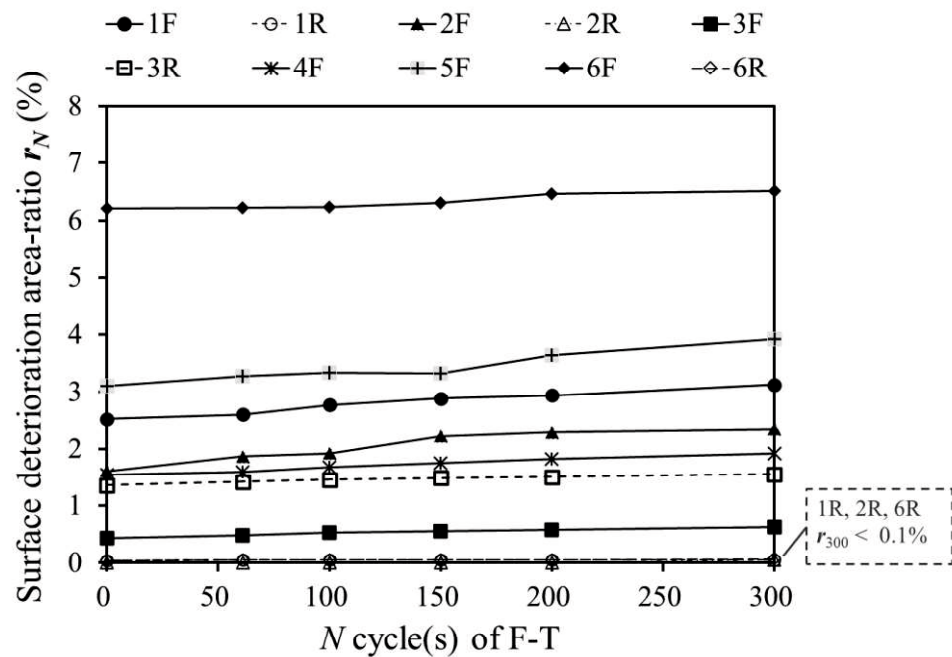
Figure 4-12 Variation of surface deterioration area-ratio during F-T cycles

Most of the sprayed water flues away along on the vertical surfaces. The retained water on the concrete surface was frozen, and its volume expanded during the F-T test. Ice water will not produce massive pressure for the bughole because the retained water in the bughole is small, and there is enough space for the expansion of ice.

After 240 cycles, the concrete specimens No.1, 2, 4, 5, and 6 were horizontally laid down with their front surface facing upwards and the bughole retained more solution. However, the variations in hole area-ratio from 0 to 100th, 100th to 200th cycle, and 200th to 300th cycle are similar. This demonstrates that the F-T test on the horizontal position from the 240th to the 300th cycle has an insignificant effect on surface deterioration. Since the bughole was opening space, the ice water will not produce massive pressure for the bughole. Therefore, the vertical and horizontal positions of specimens' surface showed a low effect on the scaling in the F-T test. Surfaces 1R, 2R, and 6R have fewer deteriorations ($r_{300} < 0.1\%$) because of their low initial bughole area-ratio.

The surface scaling area-ratio (r_{sN}), which is the increase of the deterioration area-ratio mainly caused by the microscopic scaling at the edges of bugholes, is defined below:

$$r_{sN} = r_N - r_b$$ **Equation 4-2**

Figure 4-13 shows that the scaling area-ratios were proportional to the initial bughole area-ratio. The rear surfaces of these specimens have less scaling than the front surfaces since they have less initial bughole area-ratio. It was observed that the concrete surface (1R, 2R and 6R) had less scaling during the F-T test when the initial bughole area-ratio (r_b) was lower than 0.1%. Furthermore, specimen No.1 and 2, in which air-entrained concrete was used, showed a similar surface deterioration (surface scaling < 1%) in comparison with other non-air-entrained concrete specimens. Surfaces 1F, 2F and 5F (the form angle: 30°) showed a similar initial bughole area-ratio and scaling area-ratio even in the use of a different type of concrete. It can be concluded that the scaling is hardly related to a different type of concrete and air contents which are entrapped and/or entrained air. It is remarkable that the scaling was related to the initial bughole area-ratio. Compared to a small bughole, a large one has more significant impact on F-T deterioration because the local scaling primary occurs at the edge of bughole.

Pore structures around the bughole edges, which are thin and fragile, absorb chloride water during the F-T cycles, hence it is further damaged by temperature changes. Surface bugholes increase the heterogeneous property of concrete. However,

the local scaling area-ratio is lower than 1%, and therefore not a significant influence. Consequently, a tunnel lining concrete with surface bugholes, with area-ratio lower than 5%, can be regarded as continuous and isotropic.
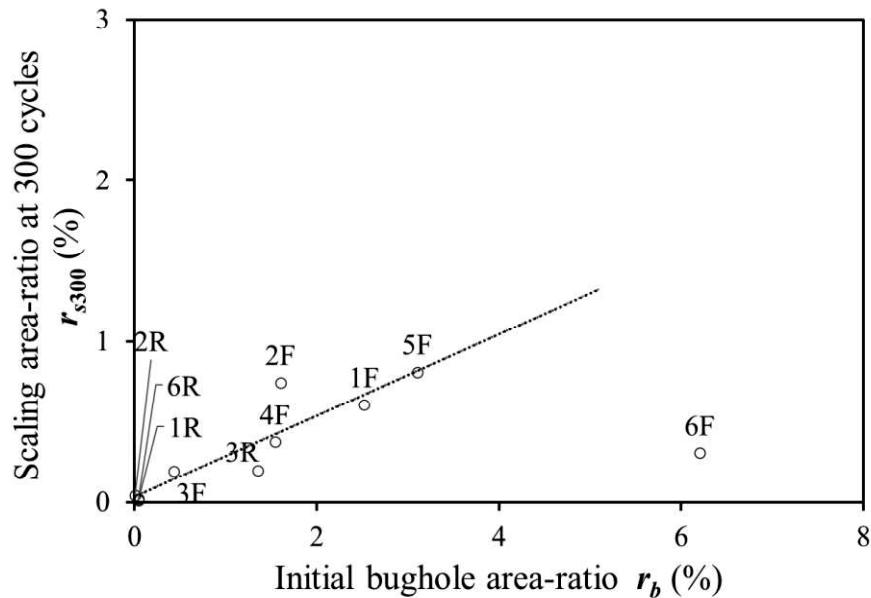
Figure 4-13 Scaling area-ratio at 300 cycles r_{s300} and initial bughole area-ratio r_b

Figure 4-14 shows the variation of surface deterioration on surface 1F, where the surface holes are isolated based on nominal diameter. The graph illustrates that both the number and area values of holes show variance among different diameter groups. If a hole enlarges or merges with other holes, the area of the hole would increase. Also, the nominal diameter would exceed the threshold value of the diameter. In such a case, the enlarged or merged hole will shift to the next larger diameter group. The enlargement and merging of the invisible bugholes (diameter < 1 mm) to visible holes (diameter 1-2 mm) increase harmful holes and significant imperfections of the surface. Although the number of holes with a diameter of over 10 mm slightly increased, the increase in area is more significant because of their larger area and longer circumference. Local scaling of cover-concrete occurs along the circumference. This relation was also observed in other concrete surfaces. Further research on the deterioration around the bughole circumference can give us more information about concrete durability.
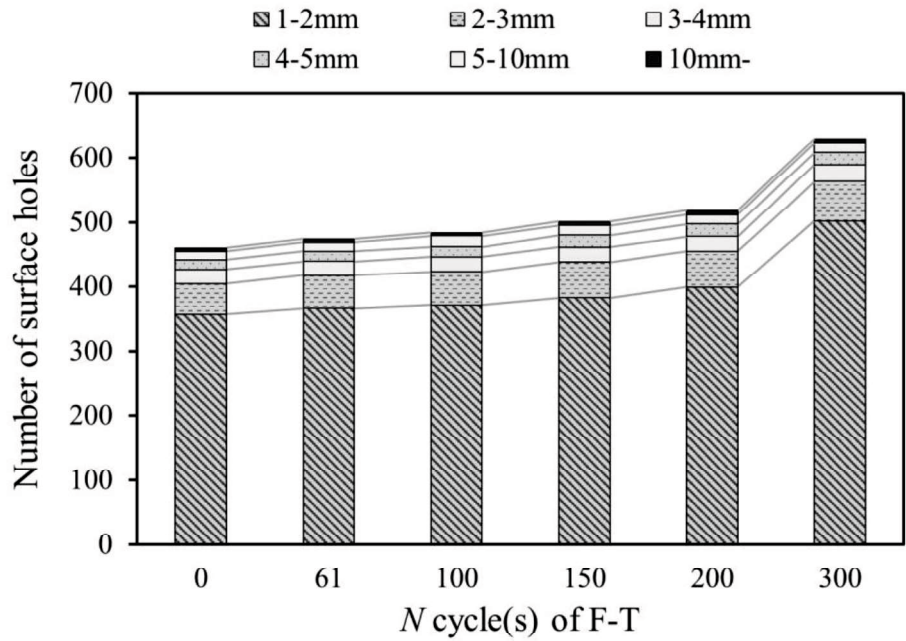
(a) number of surface holes during 300 F-T cycles
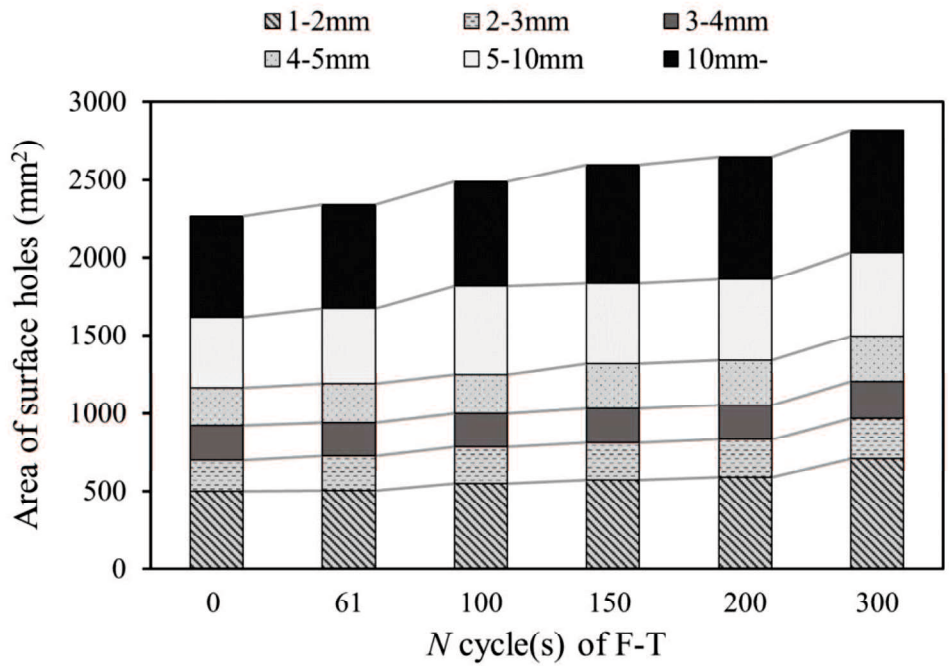
(b) hole area on surface 1F during 300 F-T cycles

Figure 4-14 Surface deterioration on surface 1F

4.5.3 Chloride penetration depth

The penetration depth of chloride at the evaluated area was determined after 300 F-T cycles using 0.1 mol/L silver nitrate solution. When the concrete contains chloride ions, the chloride binds with silver to create silver chloride, a whitish substance. In the lack of chloride, the silver combines with the hydroxides present in the concrete, resulting in a brownish color (Otsuki *et al.*,1993).

Figure 4-15 shows the position of chloride profile determined at the height of 300 mm and an image analysis area of A_2 (100 mm × 300 mm). Considering that the penetration depth of chloride is less than 50 mm, the area A_2 for the image analysis was selected as 50 mm offset from the chloride profile position. **Figure 4-16** shows the relation between penetration depth and surface bughole area ratio R_{A2}, which indicates that the chloride penetration depth increases sharply when the surface bughole area ratio is over 0.3%. The maximum penetration depth of all specimens was 40 mm. It should be noted that the chloride penetration may not be a serious concern as the thickness of concrete cover at the entrance of tunnel lining, which is constructed as RC structure, is greater than 40 mm.
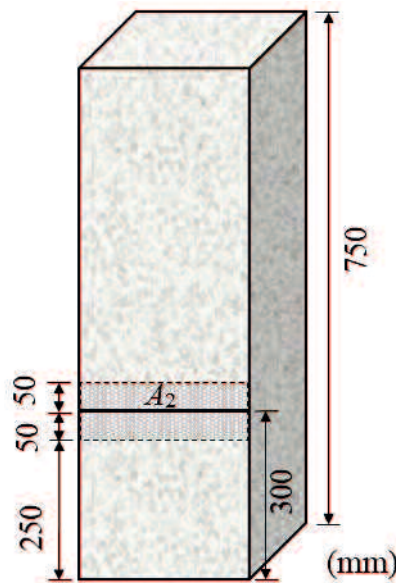
Figure 4-15 Chloride profile height and analyzed surface area A_2
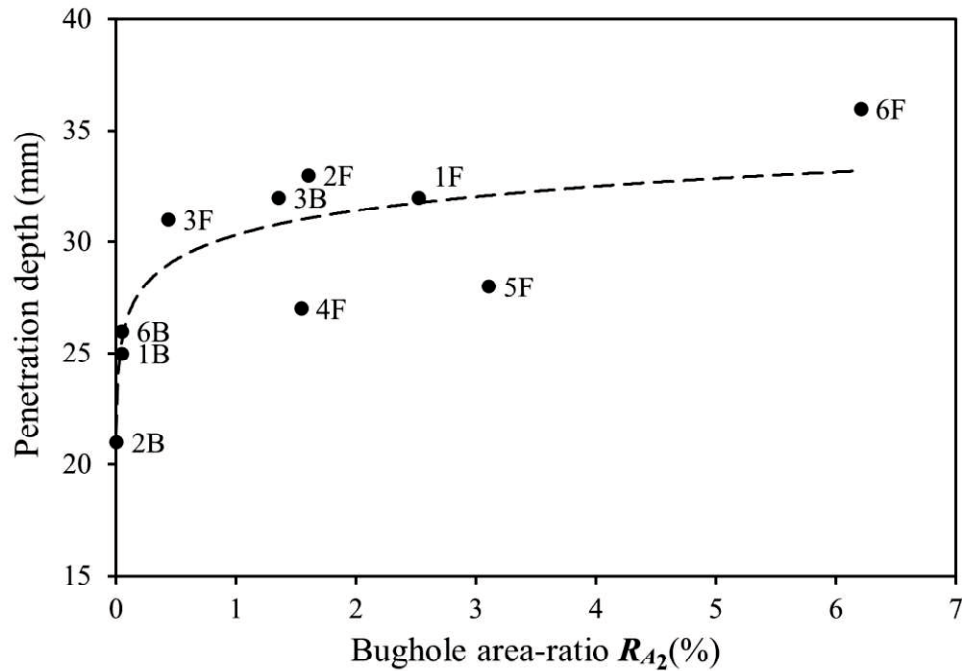
Figure 4-16 Chloride penetration depth - surface bughole area-ratio R_{A2}

4.6 SUMMARY AND CONCLUSIONS

This chapter focused on the frost durability of concrete with surface bugholes. To confirm the effect of surface bugholes on frost durability of the sidewall, a laboratory F-T test on the vertical surfaces of six lining concrete specimens was performed for 300 F-T cycles. The surface degradation was quantitatively evaluated using image analysis. The conclusions of this chapter are summarized as follows:

(1) There was a strong relationship between the formation of bugholes with the casting angle of the form. In addition, this relation depended on the types of concrete. The higher angle of tilting form, the more bugholes might appear. Ready-mixed concrete had fewer surface bugholes than site-mixed concrete.

(2) In an unsaturated chloride environment, the concrete with surface bugholes showed significant scaling at the edges of bugholes during the 300 F-T cycles. In addition, some bugholes enlarged and some merged in accordance with such local scaling. The invisible bugholes transformed into visible holes and pits and craters appeared on the concrete surface during the F-T cycles.

(3) The air-entrained or non-air-entrained concrete had no significant influence on the local scaling of bughole edge. In addition, the vertical and horizontal positions of specimens' surface showed a low effect on the scaling in the F-T test.

(4) Bugholes increased the heterogeneous, but tunnel lining concrete with surface bugholes with an area-ratio lower than 5% could be regarded as continuous and isotropic.

(5) The image analysis was a useful and practical technique to quantify deterioration areas such as surface bugholes and the scaling.

(6) Bugholes significantly influenced the scaling of the concrete surface. The concrete surface with an initial bughole area-ratio of 0.1% or lower showed little scaling at the concrete surface air-voids. In addition, the surface bughole area-ratio showed a linear relation with local scaling.

Note is that bugholes on other concrete structures, such as bridge piers and retaining walls, may also influence on F-T durability of the concrete. To mitigate the negative effect of bugholes discussed in this study, surface bugholes should be decreased as much as possible. It may be effective to employ more flowable concrete or self-consolidating concrete (SCC) for reducing bugholes. Surface treatment of concrete may contribute to the reduction of bugholes. In addition, the CVE image analysis used in the study cannot quantify the bughole depth and angles because it analyzes the 2-dimensional image of a concrete surface. Further researches on the bughole problems (such as the effects of angle and depth) should be done to improve the quality and durability of concrete structures, including NATM tunnels.

Chapter 5: Effect of Surface Bugholes on Chloride Penetration of Concrete Coated with penetrants

5.1 GENERAL

This chapter investigates the effect of surface bugholes on the chloride penetration of concrete coated with penetrants. Section 5.2 gives research motivation and significance. Section 5.3 presents the preparation of concrete specimens, penetrant materials, and the chloride immersion test. Section 5.4 shows the test results of water absorption and chloride penetration depth, and section 5.5 discusses the influence of surface bugholes. Section 5.6 summarizes and concludes the findings in this chapter.

5.2 RESEARCH MOTIVATION

Various surface penetrant materials are used to protect concrete from the harsh environment and to extend the service life of structures. The presence of bugholes is considered a nuisance since constructors are worried that they may bring insufficient coating applications. Hence, surface finishing and grinding are required before coating. It should be noted that the additional finishing work causes an increase in construction cost and time. Surface finishing or placing mortar into the bughole can only fill the bughole, but it still hardly prevents the concrete structures from environmental deteriorating attacks. Verma *et al.* (2013) reported that increasing concrete cover is the most appropriate way of increasing chloride resistance. However, bughole shortens the distance, which chlorides need to cross from cover-concrete to the reinforcing bar and increases superficial area.

Chapter 4 examined the effect of surface bugholes on F-T durability. The concrete specimens were under a combination of F-T cycles and salt attack. The saltwater was sprayed on the concrete surfaces with bugholes during 300 F-T cycles. After the test, the chloride penetration depth was determined. It showed that the penetration depth of chlorides increased sharply when the area-ratio of surface bughole is over 0.1%, as shown in **Figure 4-16**. Hence, further research on the effect of surface

bughole on chloride penetration is proposed, including its effect on the application of surface treatment agents.

The purpose of this chapter is to examine the effect of surface bugholes on the chloride penetration of concrete applied with surface treatments. This study did not discuss the effect of the sulfate deterioration because tunnel lining concrete seldom subjects to sulfate attack. A chloride immersion test was conducted on concrete specimens with surface holes in different diameters and applied with different treatment agents.

5.3 METHODOLOGY

A chloride immersion test was conducted on concrete specimens coated with various surface penetrants. The surface of concrete specimens had different sizes of holes.

Table 5-1 Concrete materials

Types	Symbol	Materials	Density (g/cm^3)
Cement	OPC	Ordinary portland cement [a]	3.16
Fine aggregate	S	Sea sand	2.60
Coarse aggregate	G1	Crushed sandstone	2.72
		Max.-Min. Size: 20–15 mm	
	G2	Crushed sandstone	2.70
		Max.-Min. Size: 15–5 mm	
Admixture	AE-WRA	Air entraining and water reducing agent	1.0

[a] Japan industrial standard (JIS). Portland cement, JIS R 5210.

5.3.1 Materials and mixture proportion

The properties of concrete materials used in this chapter are given in **Table 5-1**. All concrete specimens were made with ordinary Portland cement (JIS R 5210). Crushed stone 20-15 mm and 15-5 mm were used as coarse aggregate. The combined air-

entraining and water-reducing agent was added in concrete. The mixture proportion and properties of concrete are given in **Table 5-2**. The water-cementitious material ratio (***w/cm***) of the concrete was 0.54, which is a general mixture proportion for tunnel lining concrete in Japan.

Table 5-2 The mixture proportion and properties of concrete

Water-cement ratio (***w/cm***)	0.54
Water (kg/m^3)	172
Cement (kg/m^3)	
OPC	319
Fine aggregate (kg/m^3)	
S	880
Coarse aggregate (kg/m^3)	
G1	464
G2	464
Admixture (kg/m^3)	
AE-WRA	0.029
Air (%)	4.3-4.6
Slump (cm)	7.0-9.0
f_{cy} (MPa)	32.4

5.3.2 Concrete specimens

To make concrete with surface holes, specimens were cast in the steel-wood forms. The wooden plate on the bottom side had the various size of round screws, as shown in **Figure 5-1**. The hole size and hole area-ratio of the specimens are given in **Table 5-3**. It was supposed that a bughole with a bigger diameter has a larger depth. In other words, small-diameter bugholes having large depth cannot appear. Therefore, to some extent, the effect of bughole size can also refer to the effect of bughole depth. Thirty-four specimens were used in the chloride immersion test. To examine the corrosion of steel reinforcement in situ, specimens No.26-34 in group P-S and N-S embedded with steel rebars, as shown in **Figure 5-2**. **Figure 5-3** shows the concrete specimens with surface holes after form removal.

Figure 5-1 Steel forms with wood plates having round screws

Table 5-3 Artificial hole size on concrete surface

Hole code	Dia. × depth (mm)	Hole area-ratio (%)
H0	N/A	0.00
H5	Φ 4.5×1.2	0.72
H7	Φ 6.9×1.9	1.68
H9	Φ 9.4×2.5	3.12
H14	Φ 14×3.7	6.93
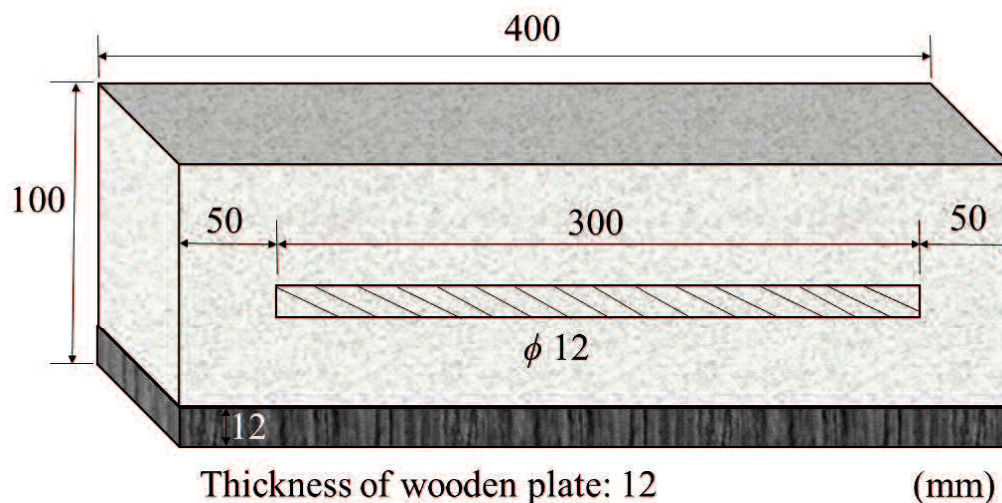
Figure 5-2 Specimen embedded with steel rebar

H5
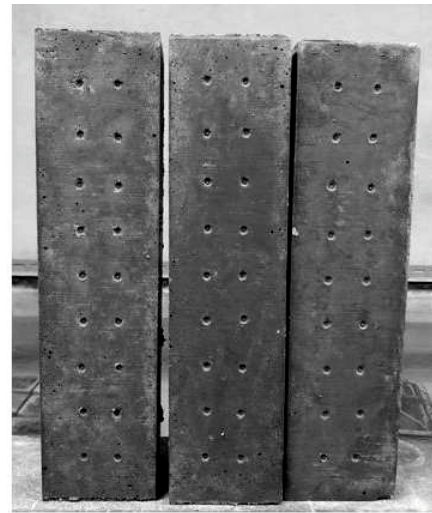
H7

H9

H14

Figure 5-3 Concrete specimens after removal of forms

5.3.3 Penetrant materials

Four types of surface coatings were used in this chapter. **Table 5-4** gives the chemical composition of surface penetrants. Type A was a kind of lithium silicate penetrant (LS), and Type B penetrant was a mixture of lithium silicate and siloxane (SO-LS). It should be noted that Type C and D were the same penetrants, a mixture of lithium silicate and silane (SA-LS), while different in coating dosage (per unit-area of concrete surface). SA-LS is a newly developed penetrant. This study aims at investigating the volume effect of the new penetrant. The composition proportion of surface penetrants is not applicable because of a contract with the manufacturer. After drying in the atmosphere for one-week, concrete surfaces were painted with penetrants

by flat brushes. Type A, B, and C were applied in a volume of 7 m²/L. The amount of penetrants liquid was enough for a specimen, and there was left penetrants liquid after first brushing. Then the specimens were brushed second time with the left penetrants. Therefore, the possibility of uneven coating can be decreased. Type D was almost double to the dosage of type C, in a volume of 3.3 m²/L. In this case, specimens were brushed four times to avoid uneven coating.

Table 5-4 Surface penetrants*

Coating type	Chemical composition	Penetrant code	Dosage (m²/liter)
A	Lithium silicate	LS	7
B	Lithium silicate Siloxane	SO-LS	7
C	Lithium silicate	SA-LS	7
D	Silane		3.3

*Manufacturer: Suruga Kogyo co. ltd.

5.3.4 Chloride immersion test

Specimens were divided into seven groups, and each group has three specimens, including two groups of uncoated specimens. **Table 5-5** gives the details of concrete specimens. All specimens were immersed in the 3% sodium chloride solution for 100 days (ASTM C-1543 and AASHTO T259).

The specimens dried in a curing room for two weeks before had been soaked in the solution. The saturated curing of concrete has a significant influence on chloride penetration, which can be decreased by the curing (Xue *et al*., 2010; Chalabi *et al*., 2017). Therefore, there is an initial sorption effect when the specimens are first exposed to the salt solution (Stanish, 2001). One hundred days are enough to determine the chloride penetration depth and to predict long-term performance. The relative amount of chloride absorbed by the capillary to the amount entering by diffusion is relatively higher within 100 days, compared to the relative quantities during the lifetime of a structure (AASHTO, 2002). Capillary absorption is the primary way of chloride penetrating the concrete in this study.

Table 5-5 Specimens used in chloride immersion test

Group	Specimen no.	Code	Hole size	Surface coating	Steel rebar
N-N	1	H0-N	H0	none	none
	2	H5-N	H5		
	3	H7-N	H7		
	4	H9-N	H9		
	5	H14-N	H14		
A-N	6	H0-A	H0	A	none
	7	H5-A	H5		
	8	H7-A	H7		
	9	H9-A	H9		
	10	H14-A	H14		
B-N	11	H0-B	H0	B	none
	12	H5-B	H5		
	13	H7-B	H7		
	14	H9-B	H9		
	15	H14-B	H14		
C-N	16	H0-C	H0	C	none
	17	H5-C	H5		
	18	H7-C	H7		
	19	H9-C	H9		
	20	H14-C	H14		
D-N	21	H0-D	H0	D	none
	22	H5-D	H5		
	23	H7-D	H7		
	24	H9-D	H9		
	25	H14-D	H14		
P-S	26	H0-A-S	H0	A	yes
	27	H0-B-S	H0	B	
	28	H0-C-S	H0	C	
	29	H0-D-S	H0	D	
N-S	30	H0-N-S	H0	none	yes
	31	H5-N-S	H5		
	32	H7-N-S	H7		
	33	H9-N-S	H9		
	34	H14-N-S	H14		

The absorbed water was determined by weighing the specimens at 1, 3, 7, 14, 21, 56, and 100 days. The water absorption ratio equals to the weight ratio of the absorbed water and concrete specimen.

After the immersion test, chloride penetration depth was measured. Specimens were cut into four blocks. Each specimen had six cutting cross-sections. Then 0.1 mol/L silver nitrate solution was used to determine the chloride outline at six cutting sections of each specimen. The average depth of chloride penetration was determined based on the discoloured section of six saw-cut sections.

5.4   TEST RESULTS

The water-repellent effect and chloride resistance of surface penetrants are discussed in the section.

5.4.1 Water absorption ratio

Figure 5-4 shows the water absorption ratio of concrete specimens during the immersion test. Group A-N has similar water absorption with uncoated group N-N, which indicates that surface penetrant LS has little resistance to water. Although specimens in group B-N displayed lower water absorption than group N-N, the water-repellent effect of siloxane-based penetrant SO-LS is questionable.
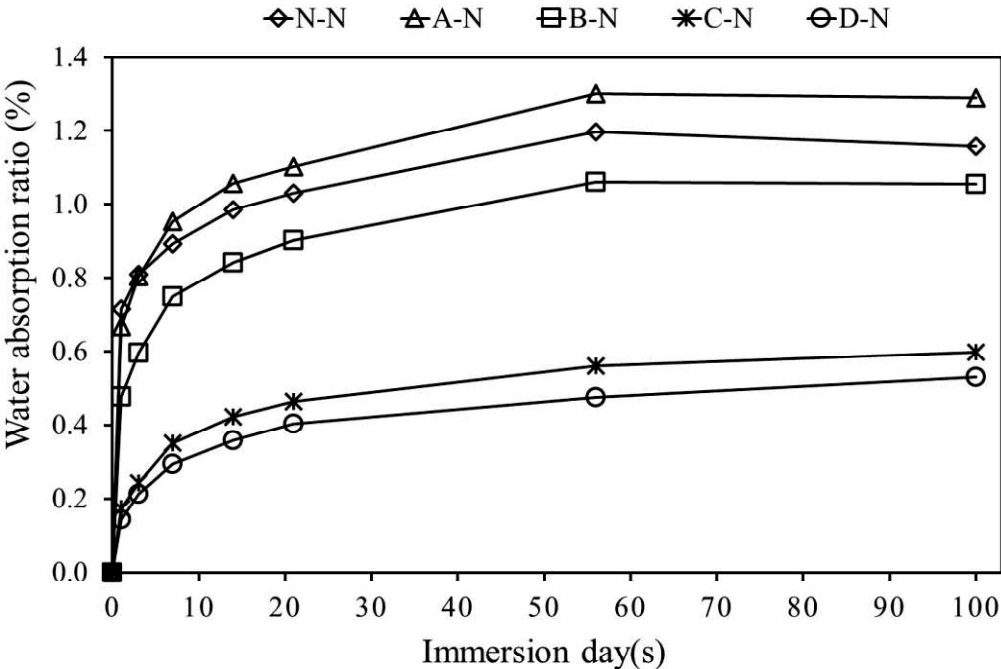

Figure 5-4 Water absorption ratio of concrete applied with different surface penetrants during immersion test

Penetrant SA-LS shows a high performance of water inhibition. This result indicates that silane is more effective than siloxane to penetrate concrete pores and make concrete resistant to water and ions. Li et al. (2012) reported that a silane-based penetrant could provide a hydrophobic surface in addition to the substrate surface tougher. The report showed that the silane was also effective to decrease cracking and to heal cracks of smaller than 0.2 mm. The interaction of silane and lithium silicate makes the concrete surface more water-repellent. Compared with a regular dosage in group C-N, double dosage of penetrant SA-LS in group D-N exhibited better water-repellent and reduced 6.7% water absorption at 100 days.

5.4.2 Chloride penetration depth

Figure 5-5 shows the chloride penetration depth of each group after 100 days of immersion test. The results indicate that surface penetrants LS and SO-LS almost have no inhibition effect for chlorides compared with group N-N. Silane penetrant SA-LS shows an excellent inhibition effect for chloride. A double dosage (group D-N) brings a double effect against chloride intruding compared with group C-N.
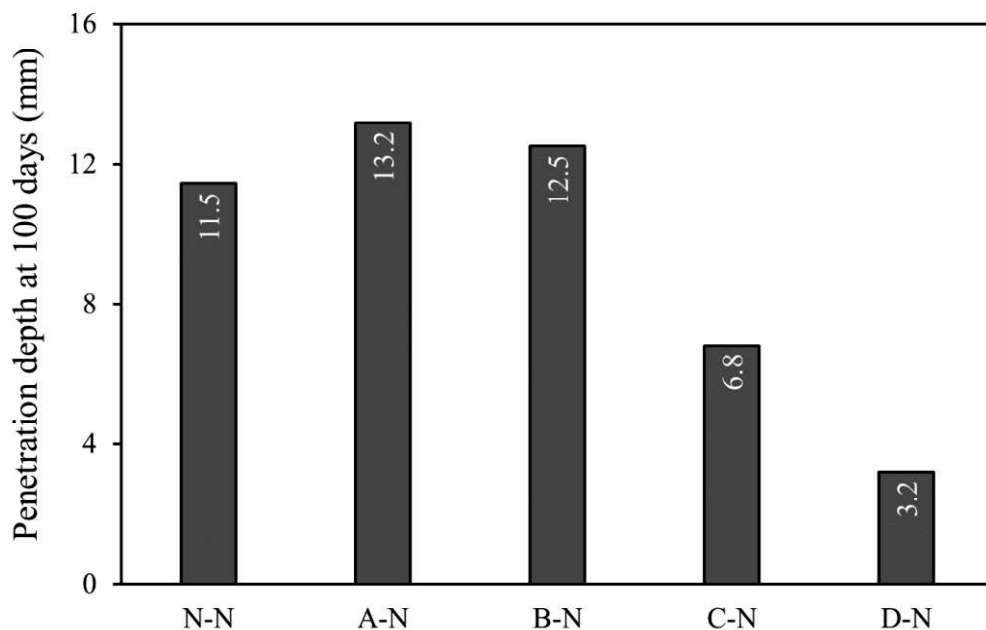

Figure 5-5 Chloride penetration depth after 100 days of immersion

Specimens in group N-S and P-S embedded steel rebar. It is supposed that chloride ions ingress into concrete and reach a certain concentration necessary to trigger corrosion of the steel reinforcement (Angst *et al.*, 2009; Apostolopoulos *et al.*,

2013; Xia *et al.*, 2020). Although bughole reduces the distance that chloride needs to across to reach reinforcement, steel corrosion did not occur in this study. The result indicates that the existence of surface bughole will not significantly degrade the structural performance.

The water absorption and chloride penetration depth of concrete groups at 100 days are shown in **Figure 5-6**. It indicates that water absorption and chloride penetration depth are highly correlated. This is to say, the water-repellent effect of surface penetrants influences the chloride inhibition significantly.
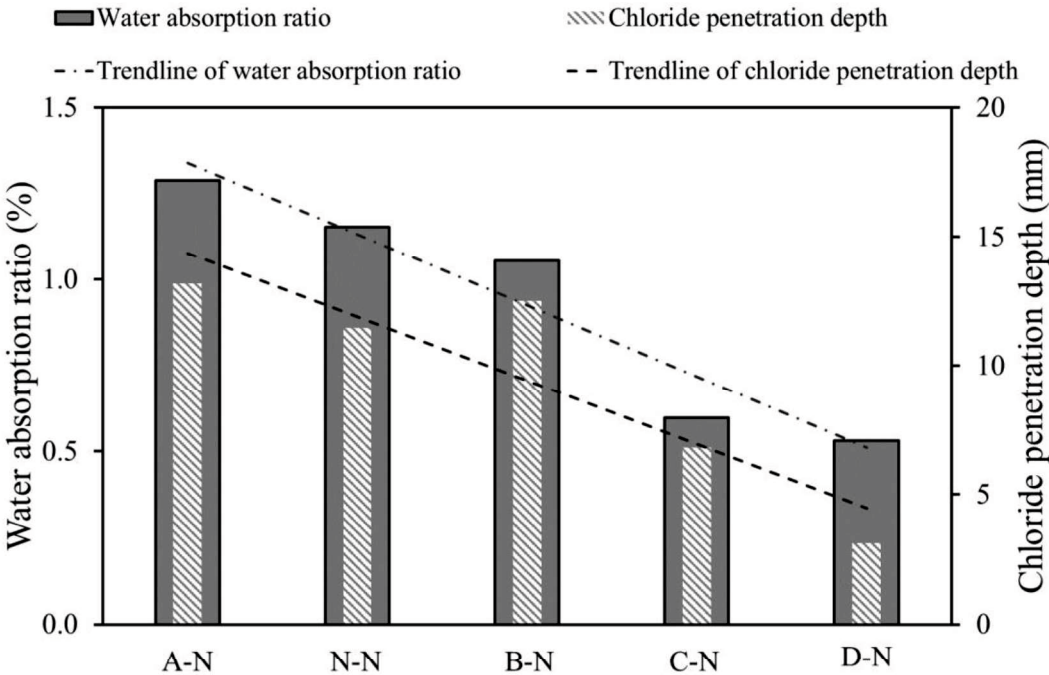
Figure 5-6 Water absorption and chloride penetration depth of concrete at 100 days

5.5 Influence of surface bugholes

Chloride penetration depth and water absorption increased with surface bughole size, in group N-N, N-S, A-N, and B-N, as shown in **Figure 5-7**(a)-(d), respectively. It shows that concrete with smaller bughole size (or lower bughole area-ratio) exhibits lower chloride penetration depth. Especially when the concrete surface is untreated (group N-N and N-S) or treated with low water-repellent penetrants (group A-N and B-N). Therefore, it can be concluded that surface bugholes have a negative effect on chloride penetration.

In contrast, group C-N and D-N show low water absorption as well as chloride penetration, as shown in **Figure 5-7** (e)-(f). However, chloride penetration depth or water absorption ratio is irregular with the surface bughole size or area-ratio. It demonstrates that silane-based penetrant SA-LS can improve water resistance effectively and against chloride intruding, even on a concrete surface with bugholes. Therefore, it can be concluded that bugholes on a concrete surface have a negligible effect on chloride intruding when the water-repellent effect of surface penetrants can be ensured. Thus, the process of surface finishing due to bugholes can be omitted before coating, which contributes to the reduction of construction cost and duration.
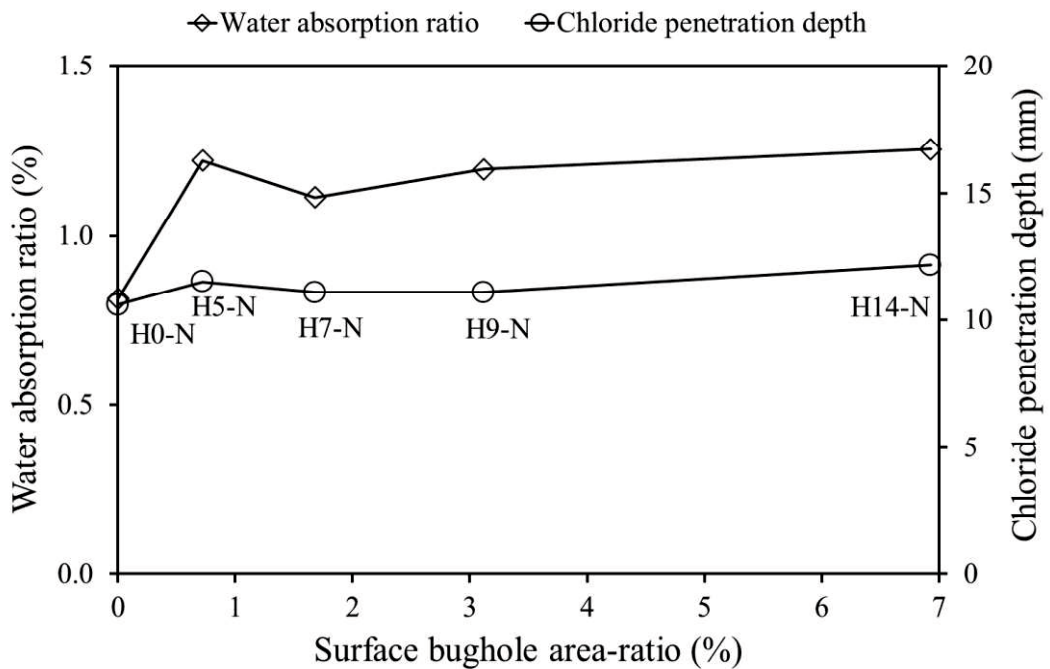
(a) group N-N
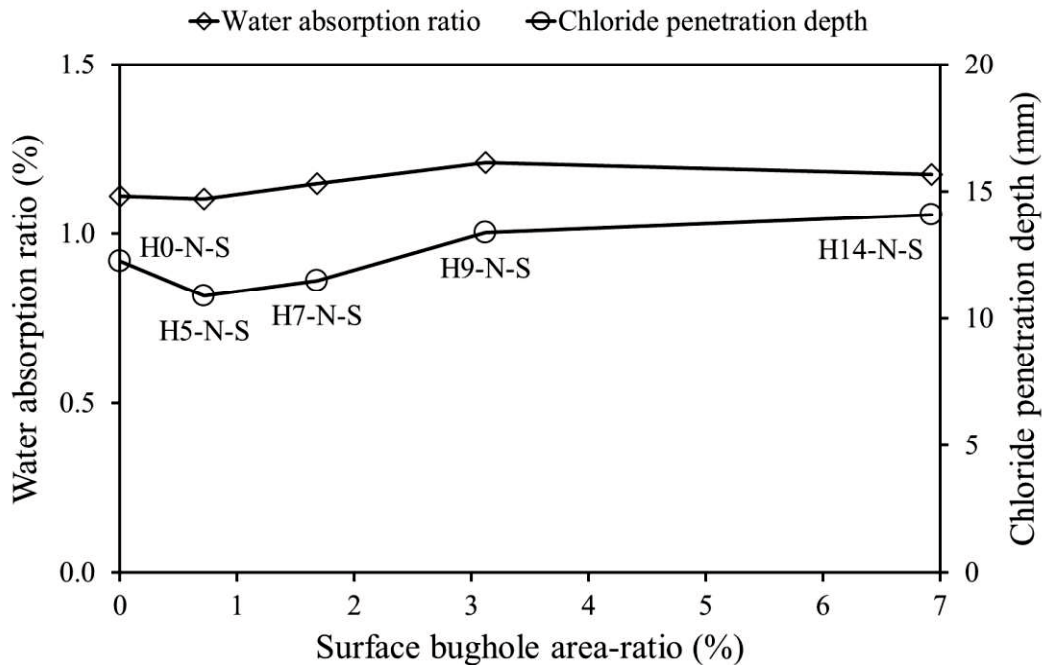
(b) group N-S
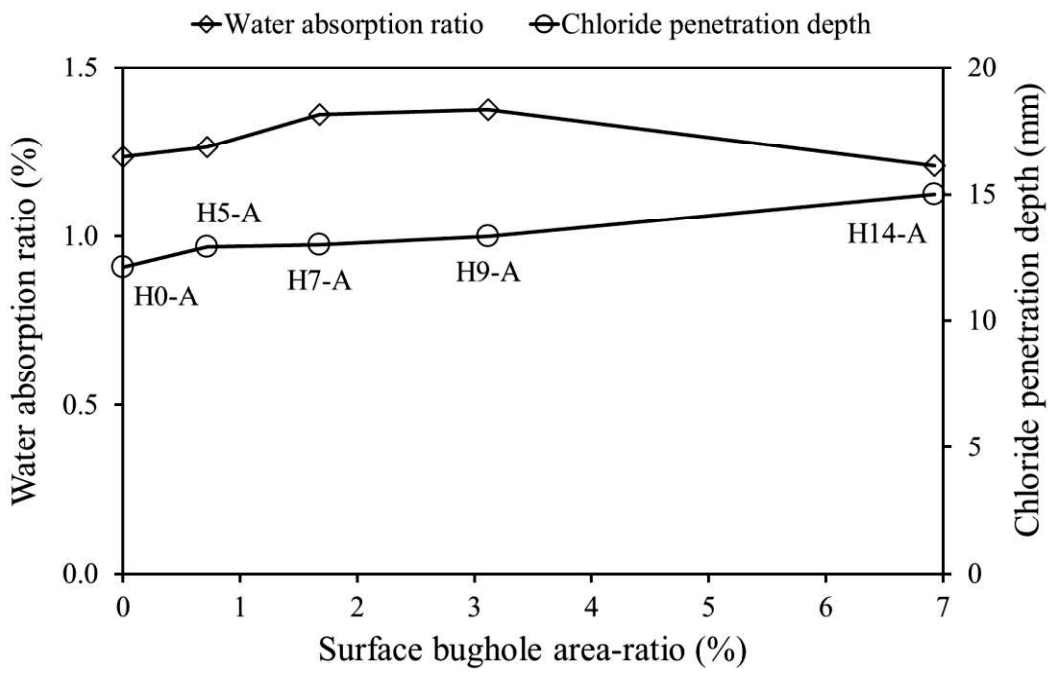
(c) group A-N
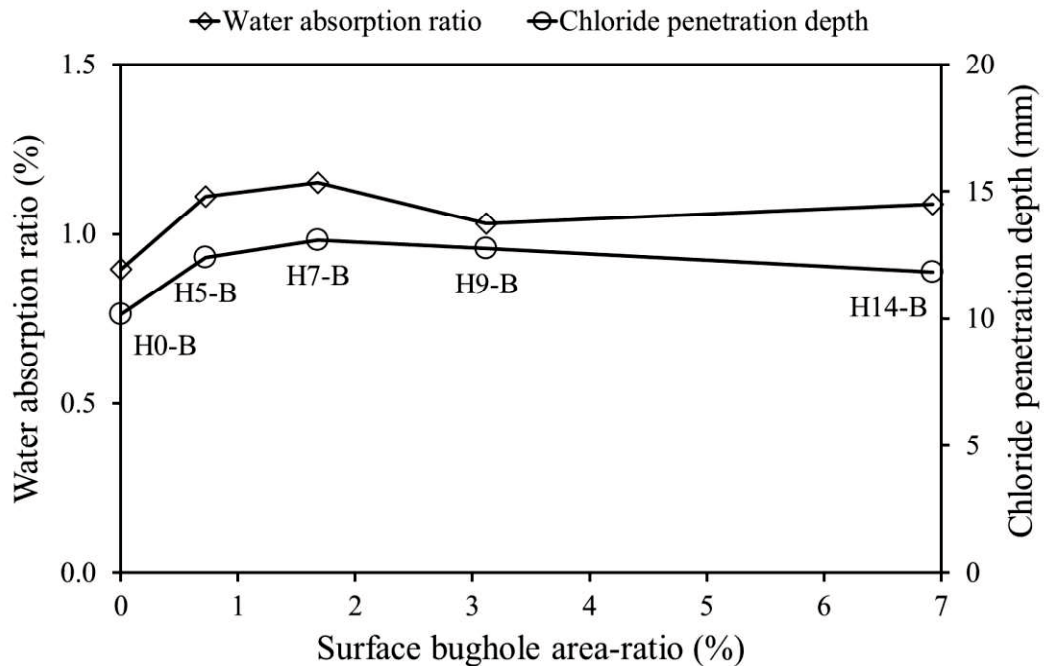
(d) group B-N
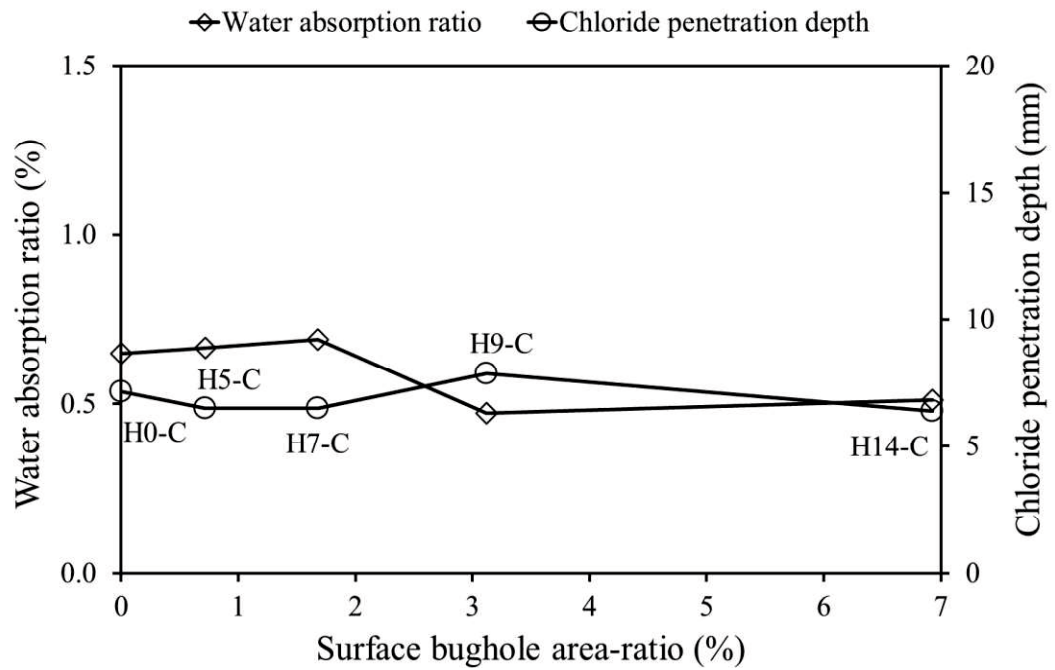
(e) group C-N
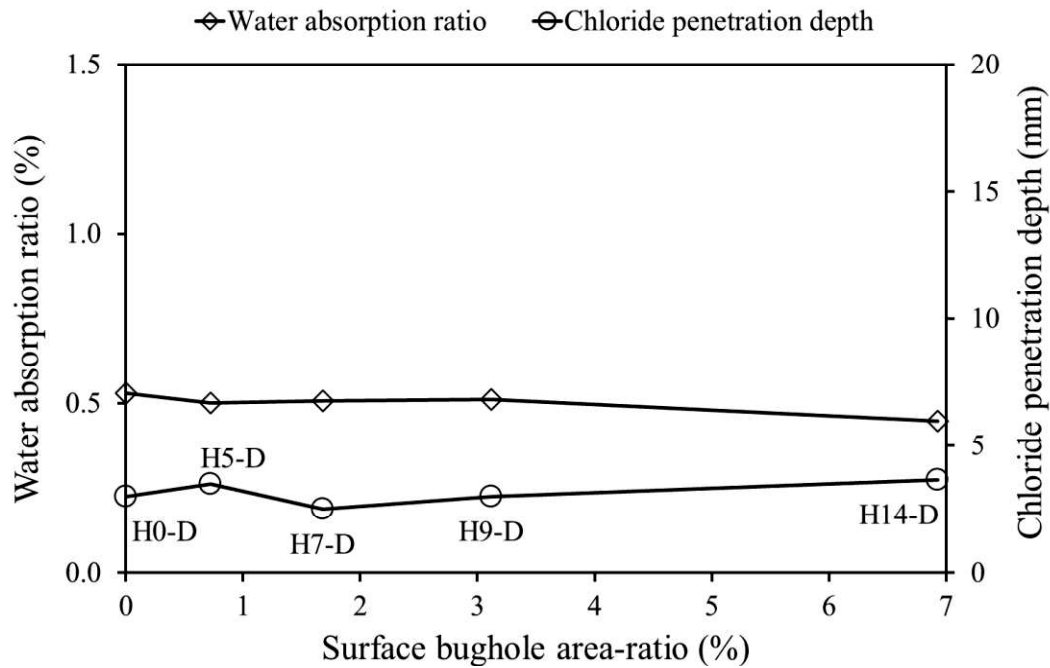
(f) group D-N

Figure 5-7 Relation of surface bughole area-ratio, water absorption, and chloride penetration depth

5.6   SUMMARY AND CONCLUSIONS

This chapter investigated the influence of surface bugholes on the effect of surface penetrants for chloride blocking. An immersion test was conducted on concrete with surface bugholes in the 3% sodium chloride solution for 100 days. The following conclusions can be drawn based on the experimental results. The following conclusions can be drawn based on the experimental results:

(1) The penetrant LS and SO-LS had low water-repellent performance, which equaled to concrete without coating.

(2) For uncoated concrete or concrete applied with low water-repellent penetrants, the water absorption and chloride penetration were highly correlated. In this case, both water absorption and chloride penetration increased with surface bugholes area-ratio.

(3) Silane-based surface penetrant SA-LS showed the high performance of water repellent and chloride inhibition. It was effective in blocking capillary pores and

against water. Double dosage of penetrant SA-LS achieved a dual suppressing chloride effect.

(4) Even applied to concrete with various sizes of surface bugholes, silane-based penetrant SA-LS was effective in blocking capillary pores and against water. Thus, the influence of surface bugholes on chloride intruding was negligible when the water-repellent effect of penetrants can be assured.

The surface substrate significantly influences on the effects of penetrants. The surface finishing due to bugholes is not a necessary process before coating. The omission of surface finishing benefits to construction efficiency and cost-cutting and hardly influences the concrete coating. Further researches on the bughole problems (such as the effects of depth) should be done to improve the quality and durability of concrete structures.

Chapter 6: Conclusions and Recommendations

6.1 GENERAL

This chapter summarizes the major findings and conclusions drawn from the current investigation, although the outcomes have been included in each chapter, respectively. In addition, the recommendations have been provided based on the results of this study. The scope for future studies, which could relieve the influence of surface bugholes, has been included in the present chapter.

6.2 CONCLUSIONS

The research objects in this study were lining concrete at the tunnel portal. The effect of surface bugholes on F-T durability and chloride penetration of tunnel lining concrete were investigated in this study. The local scaling on the concrete surface and chloride penetration was significantly affected by initial surface bugholes. Bugholes on other concrete structures, such as bridge piers and retaining walls, may also influence on F-T durability of the concrete. More attention should be paid on the surface bughole.

The following are the major findings drawn from the current investigations.

(1)   The image analysis was useful for the quantification of local scaling on a concrete surface. It was applicable for detecting surface deteriorations, including invisible surface scaling under the F-T cycles.

(2)   Compared with the visual evaluation method for surface scaling due to F-T cycles, the proposed grading-scale based on the deterioration area-ratio was useful for the evaluation of surface deterioration.

(3)   The local scaling on the concrete surface was significantly affected by initial surface bugholes before the F-T test. The concrete surface with an initial bughole area-ratio of 0.1% or lower showed little scaling at the concrete surface air-voids. In addition, the local scaling showed a linear relation with the surface bughole area-ratio.

(4) The formation of surface bugholes had a strong relationship with the casting angle of the form. In addition, this relation depended on the types of concrete. The higher angle of tilting form, the more bugholes were produced. Ready-mixed concrete had fewer surface bugholes than site-mixed concrete.

(5) In an unsaturated chloride environment, the concrete with surface bugholes showed significant scaling at the edges of bugholes during the 300 F-T cycles. In addition, some bugholes enlarged and some merged in accordance with such local scaling. The invisible bugholes transformed into visible holes, and pits and craters appeared on the concrete surface during the F-T cycles.

(6) The air-entrained or non-air-entrained concrete has no significant influence on the local scaling of bughole edge. In addition, the vertical and horizontal positions of specimens' surface showed a low effect on the scaling in the F-T test.

(7) Bugholes increased the heterogeneous, but tunnel lining concrete with surface bugholes with an area-ratio lower than 5% can be regarded as continuous and isotropic.

(8) The penetrant LS and SO-LS have low water-repellent performance, which equals to concrete without coating.

(9) For uncoated concrete or concrete applied with low water-repellent penetrants, the water absorption and chloride penetration are highly correlated. In this case, both water absorption and chloride penetration increased with surface bugholes area-ratio.

(10) Silane-based surface penetrant SA-LS showed the high performance of water repellent and chloride inhibition. It was effective in blocking capillary pores and against water. Double dosage of penetrant SA-LS achieved a dual suppressing chloride effect.

(11) Even applied to concrete with various sizes of surface bugholes, silane-based penetrant SA-LS was effective in blocking capillary pores and against water. The influence of surface bugholes on chloride intruding is negligible when the water-repellent effect of penetrants could be assured. Thus, the surface finishing due to bugholes is not a necessary process before coating. The omission of surface finishing benefits to construction efficiency and cost-cutting.

6.3   RECOMMENDATION FOR FUTURE RESEARCH WORK

The most crucial way to minimize the influence of surface bughole is by decreasing the generation of bugholes. By now, the presence of bugholes is unavoidable. It may be effective to employ more flowable concrete or self-consolidating concrete (SCC) for reducing bugholes. The development of construction methods and new materials should be investigated to reduce bugholes and help increase the concrete surface quality.

Although in this study it was supposed that concrete with a bigger diameter has a larger depth, the relation of diameter and depth of bughole should be investigated more by newly developed technology, such as 3D scanning. The future study should establish an evaluation system based on the diameter, depth, number, and area of bugholes, which can quantitatively evaluate the concrete surface quality and can be an index of construction quality.

The protection provided by surface penetrants varies according to the condition of the concrete substrate. Although the surface finishing due to bugholes can be omitted based on the current research, it should be validated in practical applications. The future study should be done to develop a fast surface treatment method to guarantee the concrete substrate before coating. Further researches on the bughole problems should be done to improve the quality and durability of concrete structures, including NATM tunnels.

References

1. AASHTO (2002) Standard method of test for resistance of concrete to chloride ion penetration. T259-02.

2. ACI Committee 116 (2000) Cement and concrete terminology, American Concrete Institute, Farmington Hills, Mich.

3. ACI Committee 301 (2016) 301-16 Specifications for structural concrete.

4. ACI Committee 347 (2014) ACI 347R-14: Guide to formwork for concrete. American Concrete Institute, MI, USA.

5. American Concrete Institute (2010) ACI concrete terminology, Farmington Hills, MI, USA, p.81.

6. Angst U., Elsener B., Larsen C.K., and Vennesland O. (2009) Critical chloride content in reinforced concrete—a review. *Cement and concrete research*, 39(12): 1122-1138. doi: 10.1016/j.cemconres.2009.08.006.

7. Apostolopoulos C.A., Demis S., and Papadakis V.G. (2013) Chloride-induced corrosion of steel reinforcement—mechanical performance and pit depth analysis. *Construction and Building Materials*, 38: 139–146. doi: 10.1016/j.conbuildmat.2012.07.087.

8. ASTM (2002) Standard test method for determining the penetration of chloride ion into concrete by ponding. ASTM C1543-02, West Conshohocken, PA.

9. ASTM C672 / C672M-12 (2012) Standard test method for scaling resistance of concrete surfaces exposed to deicing chemicals, ASTM International, West Conshohocken, PA, USA.

10. Backstrom J.E., Burrows R.W., Mielenz R.C., and Wolkodoff V.E. (1958) Origin, evolution, and effects of the air void system in concrete: part 2-influence of type and amount of air-entraining agent. *ACI Journal*, 55(8): 261–272.

11. Basheer P., Basheer L., Cleland D.J., and Long A.E. (1997) Surface treatments for concrete: assessment methods and reported performance. *Construction and Building Materials*, 11(7): 413–429. doi: 10.1016/S0950-0618(97)00019-6.

12. Bassuoni M.T., and Rahman M.M. (2016) Response of concrete to accelerated physical salt attack exposure. *Cement and Concrete Research*, 79: 395–408. doi: 10.1016/j.cemconres.2015.02.006.

13. Benito Saorin F.J., Miñano Belmonte I., Parra Costa C., Rodriguez Lopez C., and Valcuende Paya M. (2018) QSI methods for determining the quality of the surface finish of concrete. *Sustainability*, 10(4): 931. doi: 10.3390/su10040931.

14. Bertolini L., Elsener B., Pedeferri P., Redaelli E., and Polder R.B. (2013) *Corrosion of Steel in Concrete*, Wiley-Vch, Weinheim, Germany.

15. Cairns J. (1999) Enhancements in surface quality of concrete through use of controlled permeability formwork liners. *Magazine of Concrete Research*, 51(2): 73-86. doi: 10.1680/macr.1999.51.2.73.

16. Chalabi H., Bezzar A., and Khelidj A. (2017) Chloride transport in partially saturated cementitious material: influence of hydric state and binding chloride. *Magazine of Concrete Research*, 69(21): 1103-1114. doi:10.1680/jmacr.16.00342.

17. Chen J., and Luo Y. (2008) Changing rules of temperature field for tunnel in cold area. *Journal of Traffic and Transportation Engineering,* 8(2), 44–48. doi: 10.1016/j.jtte.2018.09.007.

18. Chen R., Kang E., Ji X., Yang J., and Yang Y. (2006) Cold Regions in China. *Cold Regions Science and Technology*, 45:95–102. doi: 10.1016/J.COLDREGIONS.2006.03.001.

19. CIB Working Commission W29 (1973) Tolerances on blemishes of concrete. *Concrete Surface Finishing*. CIB Report No.24. Rotterdam, Netherlands: Conseil International du Bâtiment (CIB), p. 8.

20. Çopuroğlu O., and Schlangen E. (2008) Modeling of frost salt scaling. *Cement and Concrete Research*, 38(1): 27–39. doi: 10.1016/j.cemconres.2007.09.003.

21. Delatte, N. (2009) Causes and mechanisms of deterioration in a reinforced concrete. In *Failure, Distress and Repair of Concrete Structures*. Woodhead Publishing, Cambridge, UK, pp.3–31.

22. Eymard M., Plassiard J., Perrotin P., and Le Fay S. (2015) Interfacial strength study between a concrete substrate and an innovative sprayed coating. *Construction and Building Materials*, 79: 345–356.

23. Harada S., Maeda T., Hirano M., and Yoshitake I. (2015) Reducing bug-holes on tunnel lining concrete by using covering sheets. *Proceedings of the Eighth International Structural Engineering and Construction Conference*. ISEC Press, Sydney, Australia, pp. 689–694. doi: 10.14455/ISEC.res.2015.67.

24. Hirano M., Maeda T., Honma H., Harada S., Tanase T. and Yoshitake I. (2015) Fundamental experiment for reducing bugholes on sidewall of tunnel lining concrete. *Journal of Japan Society of Civil Engineers*, Ser. F1 (Tunnel Engineering) 71: 95–105. doi: 10.2208/jscejte.71.95. (in Japanese)

25. Hirano M., Yoshitake I., Hiraoka A., and Inagawa Y. (2014) Evaluation of air bubbles distributed on concrete surface of side wall of tunnel lining. *Cement Science and Concrete Technology*, 67(1): 252–258. doi: 10.14250/cement.67.252.

26. Hiraoka A., Kakehi M., Inagawa Y., Komure H., and Yoshitake I. (2012) トンネル覆工コンクリートの仕上がりにおける美観性（見栄え）の重みについて，土木学会第67回年次学術講演会，VI-012，pp. 23-24. (in Japanese)

27. Houston B.J. (1967) Methods of reducing the size and number of voids on formed concrete surfaces. U.S. Army Engineer Waterways Experiment Station, Vicksburg, Mississippi, USA, Report No.6-788.

28. Japan Concrete Institute (2009) The standard for Portland cement, JIS R 5210.

29. JSCE (Japan Society of Civil Engineers) (2000) Tunnel concrete construction guidelines. (In Japanese)

30. Kasselouri V., Kouloumbi N., and Thomopoulos T. (2001) Performance of silica fume-calcium hydroxide mixture as a repair material. *Cement and Concrete Composites*, 23:103–110. doi: 10.1016/S0958-9465(00)00075-5.

31. Kawamura T., Mikami T., and Fukumoto K. (2008) An estimation of inner temperatures at cold region tunnel for heat insulator design. *Structural Engineering Symposium*, 54: 32–38. (in Japanese)

32. Kolymbas D. (2008) The New Austrian Tunnelling Method. In: *Tunnelling and Tunnel Mechanics: A Rational Approach to Tunnelling*. Springer Berlin Heidelberg, Berlin, Heidelberg, pp. 171–175.

33. Kozak A. (2015) Multi-criteria assessment of an acrylic coating exposed to natural and artificial weathering. Procedia Engineering, 108: 664–672.

34. Kwasny J., Sonebi M., Place J., and Amziane S. (2015) Influence of rheology on the quality of surface finish of cement-based mortars. *Construction and Building Materials*, 89: 102–109. doi: 10.1016/j.conbuildmat.2015.03.111.

35. Lemaire G., Escadeillas G., and Ringot E. (2005) Evaluating concrete surfaces using an image analysis process. *Construction and Building Materials*, 19: 604–611, doi: 10.1016/j.conbuildmat.2005.01.025.

36. Li J., Yi Z., and Xie Y. (2012) Progress of Silane Impregnating Surface Treatment Technology of Concrete Structure. *Materials Review*, 26 (3): 120–125.

37. Libessart L., Djelal C., and de Caro P. (2014) Influence of the type of release oil on steel formwork corrosion and facing aesthetics. *Construction and Building Materials*, 68: 391–401. doi: 10.1016/j.conbuildmat.2014.06.065.

38. Liu B., and Yang T. (2017a) Image analysis for detection of bugholes on concrete surface. *Construction and Building Materials*, 137: 432–440, doi:10.1016/j. conbuildmat.2017.01.098.

39. Liu B., Yang T., and Xie Y. (2017b) Factors influencing bugholes on concrete surface analyzed by image processing technology. *Construction and Building Materials*, 153: 897–907. doi: 10.1016/j.conbuildmat.2017.07.156.

40. Li G., Yang B., Guo C., Du J., and Wu X. (2015) Time dependence and service life prediction of chloride resistance of concrete coatings. *Construction and Building Materials*, 83: 19–25.

41. Liu Z., Hansen W., and Wang F. (2018) Pumping effect to accelerate liquid uptake in concrete and its implications on salt frost durability. *Construction and Building Materials*, 158: 181–188. doi: 10.1016/j.conbuildmat.2017.09.154.

42. Luo Y. (2010) Study on frost damage grades and its prevention and control technologies in cold region tunnel (Ph.D. thesis). Beijing Jiaotong University, Beijing.

43. Luo Y., and Chen J. (2019) Research status and progress of tunnel frost damage. *Journal of Traffic and Transportation Engineering* (English Ed), 6:297–309. doi: 10.1016/J.JTTE.2018.09.007.

44. Luo Y., Chen J., and Wang M. (2010) Calculation method of tunnel portal temperature based on spatial interpolation theory. China Railway Science, 31: 42–46.

45. Ma Z., Wittmann F.H., Xiao J., and Zhao T. (2016). Influence of freeze-thaw cycles on properties of integral water repellent concrete. *Journal of Wuhan University of Technology-Mater*. Sci. Ed., 31(4): 551-556, doi: 10.1007/s11595-016-1458-9.

46. Ma Z., Zhu F., and Zhao T. (2018) Effects of surface modification of silane coupling agent on the properties of concrete with freeze-thaw damage. *KSCE Journal of Civil Engineering*, 22(2): 657–669. doi: 10.1007/s12205-017-1718-z.

47. Maclnnis C., and Becaudoin J.J. (1968) Effect of degree of saturation on the frost resistance of mortar mixes. *ACI Journal*, 65(3): 203–208.

48. Maeda T., Harada S., Moriuchi M., and Yoshitake I. (2016) Reevaluation of the effect of covering sheets for reducing bugholes on tunnel lining concrete. *Proceedings of the First European and Mediterranean Structural Engineering and Construction* (Komurlu R, Gurgun AP, Singh A, Yazdani S (eds)). ISEC Press, Istanbul, Turkey, pp. 79–84.

49. Maeda T., Harada S., Moriuchi M., Fujiwara M., and Yoshitake I. (2017) Digital image analysis of concrete bugholes under vibrating consolidation. *Journal of the Society of Materials Science*, Japan, 66(3): 205–210. (in Japanese)

50. Maeda T., Honma H., Hirano M., and Yoshitake I. (2014) Permeability of tunnel lining with air/water bubbles on concrete surface. *Proceedings of the Second Australasia and South-East Asia Structural Engineering and Construction Conference*, Bangkok, Thailand, pp. 321–326. doi: 10.14455/ISEC.res.2014.32.

51. Mehta P.K., and Monteiro P.J.M. (2006) *Concrete: microstructure, properties, and materials, Concrete*. McGraw-Hill, New York, USA.

52. Meier S.J., and Wittmann F.H. (2011) Recommendation for water repellent surface impregnation of concrete. *Int. J. Restoration of Buildings and Monuments*, 17:347–358. doi: 10.1515/rbm-2011-6476.

53. MOHURD (Ministry of Housing and Urban-Rural Development) (2009) Technical specification for fair-faced concrete construction, JGJ169-2009. (in Chinese)

54. Moon H.Y., Shin D.G., and Choi D.S. (2007) Evaluation of the durability of mortar and concrete applied with inorganic coating material and surface treatment system. *Construction and Building Materials*, 21:362–369. doi: 10.1016/j.conbuildmat.2005.08.012.

55. Neville A.M. (1996) *Properties of concrete*, 4th ed. Essex, UK, Longman, p.844.

56. Otsuki N., Nagataki S., and Nakashita K. (1993) Evaluation of the AgNO$_3$ solution spray method for measurement of chloride penetration into hardened cementitious matrix materials. *Construction and Building Materials*, 7:195–201. doi: 10.1016/0950-0618(93)90002-T.

57. Ozkul T. and Kucuk I. (2010) Design and optimization of an instrument for measuring bughole rating of concrete surfaces. *Journal of the Franklin Institute*, 348(7): 1377–1392. doi: 10.1016/j.jfranklin.2010.04.004.

58. Pan X., Shi Z., Shi C., Ling T-C., and Li N. (2017a) A review on concrete surface treatment Part I: Types and mechanisms. *Construction and Building Materials*, 132:578–590. doi: 10.1016/j.conbuildmat.2016.12.025.

59. Pan X., Shi Z., Shi C., Ling T-C., and Li N. (2017b) A review on surface treatment for concrete – Part 2: Performance. *Construction and Building Materials*, 133:81–90. doi: 10.1016/j.conbuildmat.2016.11.128.

60. Park S.S., Kim Y.Y., Lee B.J., and Kwon S.J. (2014) Evaluation of concrete durability performance with sodium silicate impregnants. *Advances in Materials Science and Engineering*, 2014. doi: 10.1155/2014/945297.

61. Peterson K., Carlson J., Sutter L., and Van Dam T. (2009) Methods for threshold optimization for images collected from contrast enhanced concrete surfaces for air-void system characterization. *Material Characterization*, 60(7): 710–715. doi: 10.1016/J.MATCHAR.2008.10.005.

62. Pigeon M., Marchand J., and Pleau R. (1996) Frost resistant concrete. *Construction and Building Materials*, 10(5 SPEC. ISS.): 339–348. doi: 10.1016/0950-0618(95)00067-4.

63. Pistilli M.F. (1983) Air-void parameters developed by air-entraining admixtures, as influenced by soluble alkalies from fly ash and Portland cement. *ACI Journal*, 80(3): 217–222.

64. Popovics S. (1973) A review of the concrete consolidation by vibration. *Materials and Structures*, 6(6): 453–463. doi: 10.1007/BF02473784.

65. Powers T.C., and Helmuth R.A. (1953) Theory of volume changes in hardened Portland-cement paste during freezing. *Proceedings of the Thirty-Second Annual Meeting of the Highway Research Board* (Burggraf F, Miller WJ (eds)). Highway Research Board, Washington, D.C., USA, 285–297.

66. Price W.F., and Widdows S.J. (1991) The effects of permeable formwork on the surface properties of concrete. *Magazine of Concrete Research*, 43(1): 93–104. doi: 10.1680/macr.1991.43.155.93.

67. Rashidi A., Sigari M.H., Maghiar M., and Citrin D. (2016) An analogy between various machine-learning techniques for detecting construction materials in digital images. *KSCE Journal of Civil Engineering*, 20(4): 1178–1188. doi: 10.1007/s12205-015-0726-0.

68. RDA (Road Development Authority) and JICA (Japan International Cooperation Agency) (2018) Guideline for design of road tunnel, JICA Report.

69. Reading T.J. (1972) The bughole problem. *ACI Journal*, 69(3): 165–171.

70. RILEM Technical Committees (1993) 117-FDC Freeze-thaw and deicing resistance of concrete. *Report of the 6th Meeting in Quebec*. Canada, August.

71. Sadowski Ł., and Mathia T.G. (2016) Multi-scale metrology of concrete surface morphology: fundamentals and specificity. *Construction and Building Materials*, 113: 613–621. doi: 10.1016/J.conbuildmat.2016.03.099.

72. Samuelsson P. (1970) Voids in concrete surface. *ACI Journal*, 67(11): 868–874. doi: 10.14359/7316.

73. Setzer M.J. (1997) Basis of testing the freeze-thaw resistance: surface and internal deterioration. *Frost resistance of concrete* (Setzer M.J., Auberg R. (Eds.)), E&FN Spon, London, 157-173.

74. Setzer M.J., Fagerlund G., and Janssen D.J., (1996) CDF test—test method for the freeze-thaw resistance of concrete-tests with sodium chloride solution (CDF). *Materials and Structures*, 29(November): 523–28.

75. Shyha I., Richardson A., Coventry K., and Ponton H. (2016) Mould release technologies with regard to concrete surface finish. *Magazine of Concrete Research*, 68(2): 87-98. doi: 10.1680/macr.15.00067.

76. Silva W.R.L., and Štemberk P. (2013) Expert system applied for classifying self-compacting concrete surface finish. *Advances in Engineering Software*, 64:47–61. doi: 10.1016/J.ADVENGSOFT.2013.04.005.

77. Silva W.R.L., Lucena D.S., Štemberk P., and Prudêncio L.R. (2014) Evaluation of the effect of concrete compositional changes and the use of ethyl-alcohol and biodegradable-oil-based release agents on the final surface appearance of self-compacting concrete precast elements. *Construction and Building Materials*, 52: 202–208. doi: 10.1016/j.conbuildmat.2013.10.102.

78. Stamenkovic H. (1973) Causes, mechanisms and control of surface voids in concrete. *Materials and Structures*, 6(2): 153–154. doi: 10.1007/BF02475150.

79. Stanish K.D., Hooton R.D., and Thomas M.D.A. (2001) Testing the chloride penetration resistance of concrete: a literature review. Federal Highway Administration, United States, FHWA Contract DTFH61-97-R-00022.

80. Suleiman A.R., Soliman A.M., and Nehdi M.L. (2014) Effect of surface treatment on durability of concrete exposed to physical sulfate attack. *Construction and Building Materials*, 73: 674–681. doi: 10.1016/j.conbuildmat.2014.10.006.

81. The SCC European Project Group (2005) The European guidelines for self-compacting concrete – specification, production and use.

82. Thompson M.S. (1969) Blowholes in concrete surfaces. *Concrete*, 3(2): 64–66.

83. Valenza J.J., and Scherer G.W. (2006) Mechanism for salt scaling. *Journal of the American Ceramic Society*, 89(4): 1161–1179. doi: 10.1111/j.1551-2916.2006.00913.x.

84. Valenza J.J., and Scherer G.W. (2007a) A review of salt scaling: I. Phenomenology. *Cement and Concrete Research*, 37: 1007–1021. doi: 10.1016/j.cemconres.2007.03.003.

85. Valenza J.J., and Scherer G.W. (2007b) Mechanism for salt scaling of a cementitious surface. *Materials and Structures*, 40(3): 259–268. doi: 10.1617/s11527-006-9104-1.

86. Verma S.K., Bhadauria S.S., and Akhtar S. (2013) Evaluating effect of chloride attack and concrete cover on the probability of corrosion. *Frontiers of Structural and Civil Engineering*, 7(4): 379–390. doi: 10.1007/s11709-013-0223-9.

87. Wittmann F.H. (2007) Effective chloride barrier for reinforced concrete structures in order to extend the service-life. *Modern statistical methods for accessing the hardening process of concrete*, pp. 427–437, doi: 10.1007/978-3-540-72448-3_43.

88. Xia J., Shen J., Li T., and Jin W.L. (2020) Corrosion prediction models for steel bars in chloride-contaminated concrete: a review. *Magazine of Concrete Research.* doi: 10.1680/jmacr.20.00106.

89. Xue W., Jin W., and Yokota H. (2010) Influence of initial curing conditions and exposure environments on chloride migration in concrete using electrochemical method. *Frontiers of Architecture and Civil Engineering in China*, 4(3): 348–353. doi: 10.1007/s11709-010-0077-3.

90. Yao G., Wei F., Yang Y., and Sun Y. (2019) Deep-learning-based bughole detection for concrete surface image. *Advances in Civil Engineering*, Vol.2019. doi: 10.1155/2019/8582963.

91. Yoshitake I., Hieda M., Okamoto K., and Maeda T. (2019) Visible Test on Bughohe Generation of Fluidity Concretes for Tunnel Lining. *Proceedings of ISEC-10*, Chicago, doi: 10.14455/ISEC.res.2019.190.

92. Yoshitake I., Komure H., Kakehi M., Hiraoka A., and Inagawa Y. (2012) Questionnaire investigation of surface deterioration of lining-concrete in NATM tunnel. *Proceedings of the Research, Development, and Practice in Structural Engineering and Construction* (Vimonsatit V, Singh A, Yazdani S (eds)). Perth, Australia, pp. 221–225. doi: 10.3850/978-981-08-7920-4_M-4-0067.

93. Yoshitake I., Maeda T., and Hieda M. (2018) Image analysis for the detection and quantification of concrete bugholes in a tunnel lining. *Case Studies in Construction Materials*, 8: 116–130. doi: 10.1016/j.cscm.2018.01.002.

94. Yu Q., Zhang C., Dai Z., Du C., Mohamad Soltanian M.R., and Soltanian M. (2019) Impact of tunnel temperature variations on surrounding rocks in cold regions. *Periodica Polytechnica Civil Engineering*, 63(1): 160–167. doi: 10.3311/ppci.13109.

95. Yu S. N., Jang J. H., and Han C. S. (2007) Auto inspection system using a mobile robot for detecting concrete cracks in a tunnel. *Automation in Construction*, 16: 255–261. doi: 10.1016/j.autcon.2006.05.003.

96. Zhu Y-G., Kou S-C., Poon C-S., Dai J-G., and Li Q-Y. (2013) Influence of silane-based water repellent on the durability properties of recycled aggregate concrete. *Cement and Concrete Composites*, 35:32–38. doi: 10.1016/J.CEMCONCOMP.2012.08.008.

97. Zhu Z., and Brilakis I. (2008) Detecting air pockets for architectural concrete quality assessment using visual sensing. *Journal of Information Technology in Construction*, 13: 86–102.

98. Zhu Z., and Brilakis I. (2010) Machine vision-based concrete surface quality assessment. *Journal of Construction Engineering and Management*, 136(2): 210–218. doi: 10.1061/(ASCE)CO.1943-7862.0000126.

99. Zou D. (2016) *Theory and Technology of Rock Excavation for Civil Engineering*, Springer, Singapore.

List of Publications

1. Journal paper

a. Liangjun Hu, Isamu Yoshitake, and Tomoyuki Maeda. A laboratory test on the effect of bugholes on surface degradation of tunnel lining concrete subject to freeze-thaw cycles. *Magazine of Concrete Research*, 2020.5.

2. Conference paper (reviewed)

a. Liangjun Hu, Isamu Yoshitake, and Tomoyuki Maeda. Image analysis for quantification of local scaling on concrete surface. *The 9th International Conference on Geotechnique, Construction Materials and Environment*, Tokyo, Japan, pp.682-687, 2019.11.

b. Masayuki Sayama, Shoichi Sayama, Koji Mitani, Liangjun Hu, and Isamu Yoshitake. Effect of surface-penetrants for concrete under freeze-thaw cycles. *The 5th Australasia and South-East Asia Structural Engineering and Construction Conference*, Christchurch, New Zealand, 2020.11.

3. Conference paper (unreviewed)

a. Hu Liangjun, Hieda Masahiro, Huang Huatao, Maeda Tomoyuki, and Yoshitake Isamu. Durability of concrete with bugholes subjected to combined degradation of freeze-thaw and chloride-attack. *1st International Conference on Durability of Building and Infrastructures (DuraBI) 2018*, Miri, Malaysia, pp.155-158, 2018.1.